# Field-induced Multi- $\vec{Q}$ States in a Pyrochlore Heisenberg Magnet

Cecilie Glittum<sup>1, 2, 3</sup> and Olav F. Syljuåsen<sup>4</sup>

<sup>1</sup> T.C.M. Group, Cavendish Laboratory, JJ Thomson Avenue, Cambridge CB3 0HE, United Kingdom

<sup>2</sup> Helmholtz-Zentrum Berlin für Materialien und Energie GmbH, Hahn-Meitner-Platz 1 14109 Berlin, Germany

<sup>3</sup> Dahlem Center for Complex Quantum Systems and Fachbereich Physik,

Freie Universität Berlin, 14195 Berlin, Germany

<sup>4</sup> Department of Physics, University of Oslo, P. O. Box 1048 Blindern, N-0316 Oslo, Norway

(Dated: March 10, 2025)

We construct exact ground states of the  $J_1$ - $J_{3b}$  classical Heisenberg model on the pyrochlore lattice in the presence of a magnetic field. They are non-coplanar multi- $\vec{Q}$  spin configurations with a large magnetic unit cell that generalize the previously found coplanar sublattice pairing states. Using linear spin wave theory, we show that entropy favors these multi- $\vec{Q}$  states at low temperatures in high magnetic fields. This is confirmed by Monte Carlo simulations, and a phase diagram is constructed. We also calculate the zero-temperature dynamical structure factor. Besides the usual Goldstone modes associated with the ordering  $\vec{Q}$ s, we find high intensity gapless modes at momenta where there are no Bragg peaks.

#### I. INTRODUCTION

Frustrated magnets, and particularly the highly frustrated pyrochlores, have garnered significant attention due to their predicted ability to host exotic states of matter, such as classical spin liquids. The antiferromagnetic (AF) nearest-neighbor Heisenberg model on the pyrochlore lattice is such a spin liquid, even down to zero temperature, due to its huge ground state degeneracy [1–4]. This degeneracy is however lifted by furtherneighbor couplings, and inclusion of second- and third-nearest neighbor couplings destabilize the spin liquid, inducing different kinds of order [5–8].

While the primary interest in frustrated magnetism often lies in the lack of magnetic order in presence of strong correlations, i.e. spin liquidity, non-coplanar ordered states with several ordering wave vectors have also gained much attention, particularly due to their applications in spintronics [9–11]. Such multi- $\vec{Q}$  states are typically known to be realized in the presence of the Dzyaloshinskii–Moriya interaction [12–14]. However, they can also be stabilized by frustration [15], particularly with additional anisotropic exchange interactions [16, 17], impurities [18] or coupling to itinerant electrons [19–21]. These mechanisms are also known to induce multi- $\vec{Q}$  states on pyrochlore lattices [5–7, 22–24].

The third nearest-neighbor couplings are predicted to be the most important further-neighbor couplings in several pyrochlore materials [25–27]. For the pure AF  $J_1$ - $J_{3b}$  Heisenberg model (see Fig. 1), coplanar sublattice pairing (SLP) states are known to minimize the  $J_1$  and  $J_{3b}$  energy terms simultaneously [8]. In these states, sublattices pair up antiferromagnetically, forming coplanar single- $\vec{Q}$  spirals corresponding to 120° order in the triangular planes formed by the  $J_{3b}$  coupling.

Here, we study the impact of an applied magnetic field on the pyrochlore AF  $J_1$ - $J_{3b}$  Heisenberg model. We start by allowing for a finite magnetization by constructing a generalized magnetic-field analog of the SLP ansatz of

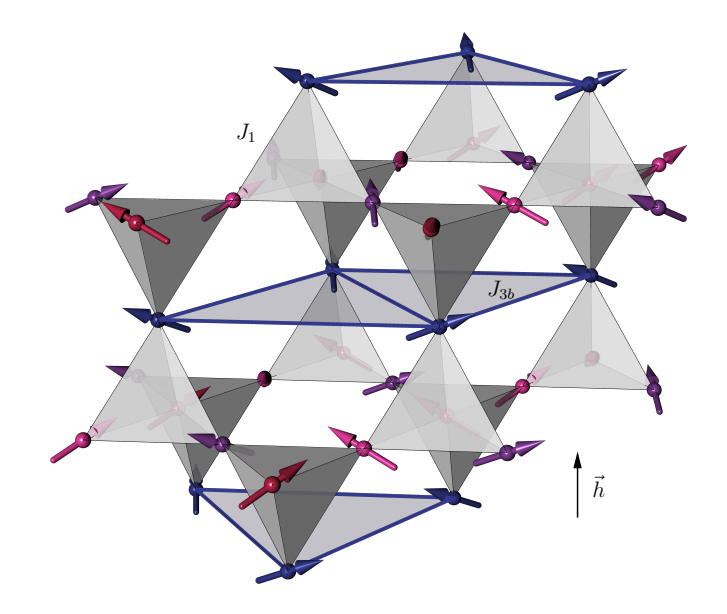


FIG. 1. The pyrochlore lattice with an example of the canted  $\operatorname{SLP}_1$  state in a magnetic field h=4. On sublattice 1 (blue), we illustrate how  $J_{3b}$  effectively couples spins in triangular planes. In the canted  $\operatorname{SLP}_1$  state, spins on pairs of sublattices form antiparallel spirals in the  $\bot$ -components (relative to the magnetic field direction), while all  $\parallel$ -components are equal. Each triangular plane on a given sublattice has the same three spins. The  $\operatorname{SLP}_1$  state can also be viewed as chains of spins with staggered  $\bot$ -components – here for chains of pink and blue spins and chains of red and purple spins.

Ref. 8. This ansatz allows for a simultaneous SLP between all pairs of sublattices, and can describe more general states than the simple single- $\vec{Q}$  spiral on each sublattice. Instead, each sublattice has up to three ordering wave vectors, one for each sublattice pair. The system thus has up to six ordering wave vectors in total. We present normalized multi- $\vec{Q}$  states satisfying the ansatz, and show that a particular  $6\vec{Q}$ -state is favored entrop-

ically at sufficiently high magnetic fields. We confirm our findings using Monte Carlo (MC) simulations, and map out the finite-temperature phase diagram. Lastly, we compute the zero-temperature dynamical structure factor for selected values of the magnetic field.

#### II. HAMILTONIAN

We consider the following classical Heisenberg Hamiltonian in a magnetic field  $\vec{h}$  on the pyrochlore lattice

$$H = J_1 \sum_{\langle \vec{r}, \vec{r}' \rangle} \vec{S}_{\vec{r}} \cdot \vec{S}_{\vec{r}'} + J_{3b} \sum_{\langle \langle \langle \vec{r}, \vec{r}' \rangle \rangle \rangle_b} \vec{S}_{\vec{r}} \cdot \vec{S}_{\vec{r}'} - \sum_{\vec{r}} \vec{h} \cdot \vec{S}_{\vec{r}}, \quad (1)$$

where the AF exchange couplings  $J_1 = 1$  and  $J_{3b} > 0$  are illustrated in Fig. 1.

We begin by rewriting the Hamiltonian as

$$H = \frac{J_1}{2} \sum_{t} \left( \vec{S}_{t,0} + \vec{S}_{t,1} + \vec{S}_{t,2} + \vec{S}_{t,3} - 4\vec{m} \right)^{2} + \frac{J_{3b}}{4} \sum_{s=0}^{3} \sum_{\Delta} \left( \vec{S}_{i_0,s} + \vec{S}_{i_1,s} + \vec{S}_{i_2,s} - 3\vec{m} \right)^{2},$$
(2)

where the first sum goes over all up and down tetrahedra of the lattice, of which there are N/2 (N is the number of spins), and  $\vec{S}_{t,s}$  denotes the spin on tetrahedron number t and sublattice s. The second sum goes over all elementary triangles on the triangular lattices formed by the  $J_{3b}$  bonds, which couple spins on the same sublattice s. The number of such triangles on each sublattice is also N/2. The sites on each triangle are denoted  $i_0, i_1$ and  $i_2$ . We have subtracted a constant term coming from the spins and the average magnetization squared ( $\vec{m}$  is the average magnetization per spin). Multiplying out the parentheses, the resulting Hamiltonian is that of the  $J_1$ - $J_{3b}$  model in a magnetic field, where the magnetic field is along the axis of the magnetization and has magnitude  $h = (8J_1 + 9J_{3b}) m$ . This gives a saturation field  $h_{\rm sat} = 8J_1 + 9J_{3b}$ , and an average magnetization per spin

$$m = \frac{h}{8J_1 + 9J_{3b}}. (3)$$

The ground state energy (the constant we subtracted earlier) per spin is

$$\frac{E_{\rm GS}}{N} = -\left(J_1 + \frac{3}{2}J_{3b} + \frac{h^2}{2(8J_1 + 9J_{2b})}\right). \tag{4}$$

In Eq. (2), we have chosen to write the Hamiltonian so that the lowest energy is achieved when the spins satisfy

$$\vec{S}_{t,0} + \vec{S}_{t,1} + \vec{S}_{t,2} + \vec{S}_{t,3} = 4\vec{m} \tag{5}$$

for each tetrahedron and

$$\vec{S}_{i_0,s} + \vec{S}_{i_1,s} + \vec{S}_{i_2,s} = 3\vec{m} \tag{6}$$

for each triangle. We will refer to Eq. (5) (Eq. (6)) as the tetrahedron (triangle) condition. The rationale behind this choice is to match it with known results in the cases  $J_1 > 0$ ,  $J_{3b} = 0$  [28] and  $J_1 = 0$ ,  $J_{3b} > 0$  [29].

TABLE I. The  $\vec{Q}_{ij}$ s in terms of reciprocal lattice vectors.  $\vec{R} = n_1 \vec{a}_1 + n_2 \vec{a}_2 + n_3 \vec{a}_3$ .

$\vec{Q}_{ij}$	momentum	$ec{Q}\cdotec{R}$
$\vec{Q}_{01}$	$(\vec{b}_3 - \vec{b}_2)/3$	$(2\pi/3)\left(n_3-n_2\right)$
$\vec{Q}_{02}$	$(\vec{b}_1-\vec{b}_3)/3$	$(2\pi/3)\left(n_1-n_3\right)$
$ec{Q}_{03}$	$(\vec{b}_2 - \vec{b}_1)/3$	$(2\pi/3)\left(n_2-n_1\right)$
$\vec{Q}_{23}$	$(2\vec{b}_1 + \vec{b}_2 + \vec{b}_3)/3$	$(2\pi/3)(2n_1+n_2+n_3)$
		$(2\pi/3)(n_1+2n_2+n_3)$
$\vec{Q}_{12}$	$(\vec{b}_1 + \vec{b}_2 + 2\vec{b}_3)/3$	$(2\pi/3)(n_1+n_2+2n_3)$

#### A. Ansatz

In the following, we label the spins by either their fcc lattice point  $\vec{R}$  and sublattice index  $i=\{0,1,2,3\}$ , or their position  $\vec{r}=\vec{R}+\vec{\alpha}_i$ .  $\vec{R}$  describes the position of an up tetrahedron and is constructed from the fcc primitive lattice vectors  $\vec{a}_1=(0,1/2,1/2), \vec{a}_2=(1/2,0,1/2),$  and  $\vec{a}_3=(1/2,1/2,0),$  where we have set the cubic lattice constant to unity. The corresponding reciprocal lattice vectors are  $\vec{b}_1=2\pi(-1,1,1), \ \vec{b}_2=2\pi(1,-1,1),$  and  $\vec{b}_3=2\pi(1,1,-1).$  The sublattice vectors  $\vec{\alpha}_i$ , which describe the spin positions on a single up tetrahedron, are  $\vec{\alpha}_i=\vec{a}_i/2$  for  $i=\{0,1,2,3\}$ , where we have defined  $\vec{a}_0=(0,0,0).$ 

A general ansatz satisfying the tetrahedron and triangle conditions is

$$\begin{split} \vec{S}_{\vec{R},0} &= + \vec{u}_{01} \cos{(\vec{Q}_{01} \cdot \vec{R})} + \vec{v}_{01} \sin{(\vec{Q}_{01} \cdot \vec{R})} \\ &+ \vec{u}_{02} \cos{(\vec{Q}_{02} \cdot \vec{R})} + \vec{v}_{02} \sin{(\vec{Q}_{02} \cdot \vec{R})} \\ &+ \vec{u}_{03} \cos{(\vec{Q}_{03} \cdot \vec{R})} + \vec{v}_{03} \sin{(\vec{Q}_{03} \cdot \vec{R})} + \vec{m}, \\ \vec{S}_{\vec{R},1} &= - \vec{u}_{01} \cos{(\vec{Q}_{01} \cdot \vec{R})} - \vec{v}_{01} \sin{(\vec{Q}_{01} \cdot \vec{R})} \\ &+ \vec{u}_{12} \cos{(\vec{Q}_{12} \cdot \vec{R})} + \vec{v}_{12} \sin{(\vec{Q}_{12} \cdot \vec{R})} \\ &+ \vec{u}_{13} \cos{(\vec{Q}_{13} \cdot \vec{R})} + \vec{v}_{13} \sin{(\vec{Q}_{13} \cdot \vec{R})} + \vec{m}, \\ \vec{S}_{\vec{R},2} &= - \vec{u}_{02} \cos{(\vec{Q}_{02} \cdot \vec{R})} - \vec{v}_{02} \sin{(\vec{Q}_{02} \cdot \vec{R})} \\ &- \vec{u}_{12} \cos{(\vec{Q}_{12} \cdot \vec{R})} - \vec{v}_{12} \sin{(\vec{Q}_{12} \cdot \vec{R})} \\ &+ \vec{u}_{23} \cos{(\vec{Q}_{23} \cdot \vec{R})} + \vec{v}_{23} \sin{(\vec{Q}_{23} \cdot \vec{R})} + \vec{m}, \\ \vec{S}_{\vec{R},3} &= - \vec{u}_{03} \cos{(\vec{Q}_{03} \cdot \vec{R})} - \vec{v}_{03} \sin{(\vec{Q}_{03} \cdot \vec{R})} \\ &- \vec{u}_{13} \cos{(\vec{Q}_{13} \cdot \vec{R})} - \vec{v}_{13} \sin{(\vec{Q}_{13} \cdot \vec{R})} \\ &- \vec{u}_{23} \cos{(\vec{Q}_{23} \cdot \vec{R})} - \vec{v}_{23} \sin{(\vec{Q}_{23} \cdot \vec{R})} + \vec{m}, \end{split}$$

where the wave vectors  $\vec{Q}_{ij}$  are listed in Table I. Note that the minus signs in the ansatz cause an antiparallel tendency of spins on pairs of sublattices, hence we term this ansatz the SLP ansatz.

The choice of minus signs gives  $\vec{S}_{\vec{R},0} + \vec{S}_{\vec{R},1} + \vec{S}_{\vec{R},2} + \vec{S}_{\vec{R},3} = 4\vec{m}$ , meaning that the tetrahedron condition is satisfied for all up tetrahedra. The tetrahedron condition is also satisfied for the down tetrahedra,  $\sum_i \vec{S}_{\vec{R}-\vec{a}_i,i} = \vec{S}_{\vec{R}-\vec{a}_i,i} = \vec{S}_{\vec{R}-\vec{a}_i,i}$ 

TABLE II. The triangular basis vectors  $\vec{t}_1, \vec{t}_2$  and their "normal" vector  $\vec{n}$  on the different sublattices, as well as their plane index P and trisublattice index T. A general point  $\vec{R} = n_1\vec{a}_1 + n_2\vec{a}_2 + n_3\vec{a}_3 = P\vec{n} + m_1\vec{t}_1 + m_2\vec{t}_2$ , and  $T \equiv (m_1 + m_2) \mod 3$ . We have defined  $n_0 = -n_1 - n_2 - n_3$ . Both T and P are understood to be mod 3.

sublattice	$ec{t}_1$	$ec{t}_2$	$\vec{n}$	T	P
0	$-\vec{a}_3 + \vec{a}_1$	$-\vec{a}_1 + \vec{a}_2$	$\vec{a}_1 - \vec{a}_0$	$n_2 - n_3$	$-n_0$
1	$+\vec{a}_2-\vec{a}_0$	$+\vec{a}_0 - \vec{a}_3$	$\vec{a}_0 - \vec{a}_1$	$n_2 - n_3$	$-n_1$
2	$-\vec{a}_1 + \vec{a}_3$	$-\vec{a}_3 + \vec{a}_0$	$\vec{a}_3 - \vec{a}_2$	$n_0 - n_1$	$-n_2$
3	$+\vec{a}_0 - \vec{a}_2$	$+\vec{a}_2-\vec{a}_1$	$\vec{a}_2 - \vec{a}_3$	$n_0 - n_1$	$-n_3$

 $4\vec{m}$ . This can be seen by letting  $\vec{R} \to \vec{R} - \vec{a}_i$  on sublattice i. It gives the same cancellations as for the up tetrahedra, which follows from  $\vec{Q}_{ij} \cdot \vec{a}_i = \vec{Q}_{ij} \cdot \vec{a}_j$ , as one can easily check by inspecting Table I.

To see that also the triangle condition is satisfied, it is necessary to divide each sublattice into parallel triangular  $J_{3b}$  planes (as shown for one of the sublattices in Fig. 1), and furthermore, divide each triangular plane into trisublattices, such that an elementary triangle has one site from each trisublattice. A possible way of doing this is to introduce integer-valued plane and trisublattice indices, P and T, respectively, as defined in Table II. When rewriting the SLP ansatz in Eq. (7) with this labeling, we find that the particular choices of  $\vec{Q}_{ij}$ s in Table I cause all trigonometric functions to have arguments which depend on the trisublattice index as  $2\pi T/3$  and on the plane index as  $2\pi P/3$ . Therefore, for each elementary triangle in a given plane, the trigonometric functions from the different trisublattices cancel each other, and the triangle condition is satisfied. We also note that there are at most three different planes on a given sublattice, which follows from the  $2\pi P/3$  dependence, making the spin configuration periodic when P changes by 3.

## III. GROUND STATES

Since the SLP ansatz in Eq. (7) fulfills both the tetrahedron and triangle conditions, any proper state satisfying the ansatz is a ground state of the Hamiltonian. To be a proper classical spin state, each spin must have unit length. It is in general difficult to acheive this for multilength. It is in general difficult to acheive this for multilength states, as they often have a large number of different spins in the unit cell and a corresponding large number of normalization constraints. Here, the  $\vec{Q}_{ij}$ s make any spin configuration that obeys Eq. (7) periodic with unit cell  $(3\vec{a}_1, 3\vec{a}_2, 3\vec{a}_3)$ , with a total of 108 spins. However, only 36 of these spins can be different, nine on each sublattice (at most three different planes with three spins each on each sublattice), giving rise to 36 normalization constraints. These are listed in Appendix A.

## A. Zero field

In zero field, the simplest solution to the normalization constraints is the coplanar solution introduced in Ref. 8. It amounts to setting all  $\vec{u}$ 's and  $\vec{v}$ 's to zero except  $\vec{u}_{01} \perp \vec{v}_{01}$  and  $\vec{u}_{23} \perp \vec{v}_{23}$ , which are all unit vectors. Explicitly, it is

$$\vec{S}_{\vec{R},0} = +\vec{u}_{01}\cos(\vec{Q}_{01} \cdot \vec{R}) + \vec{v}_{01}\sin(\vec{Q}_{01} \cdot \vec{R}),$$

$$\vec{S}_{\vec{R},1} = -\vec{u}_{01}\cos(\vec{Q}_{01} \cdot \vec{R}) - \vec{v}_{01}\sin(\vec{Q}_{01} \cdot \vec{R}),$$

$$\vec{S}_{\vec{R},2} = +\vec{u}_{23}\cos(\vec{Q}_{23} \cdot \vec{R}) + \vec{v}_{23}\sin(\vec{Q}_{23} \cdot \vec{R}),$$

$$\vec{S}_{\vec{R},3} = -\vec{u}_{23}\cos(\vec{Q}_{23} \cdot \vec{R}) - \vec{v}_{23}\sin(\vec{Q}_{23} \cdot \vec{R}).$$
(8)

This corresponds to sublattice pairing (01)&(23). Other sublattice pairings ((02)&(13) and (03)&(12)) are also possible. In this state, the three coplanar spins on a particular plane and sublattice are constructed from a single wave vector  $Q_{ij}$  (and its negative) and form a 120° arrangement which is the same for all planes on the given sublattice. We call this state SLP<sub>1</sub>, where the subscript refers to the number of different momenta  $\vec{Q}_{ij}$  on each sublattice  $(\pm \vec{Q}_{ij})$  are considered equal in this respect). As a whole, SLP<sub>1</sub> is a  $2\vec{Q}$ -state, as both  $\vec{Q}_{01}$  and  $\vec{Q}_{23}$  are present. The SLP<sub>1</sub> state has the characteristic feature of antiparallel spins going along the  $\vec{a}_0 - \vec{a}_1$  and  $\vec{a}_2 - \vec{a}_3$  directions on sublattices 0, 1 and 2, 3, respectively. In Ref. 8, it was found that among the possible relative orientations of the spiral ordering vectors  $\vec{u}_{01}$  and  $\vec{u}_{23}$  $(\vec{v}_{01} \text{ and } \vec{v}_{23})$ , spin wave fluctuations selects entropically the coplanar state  $\vec{u}_{01} = \vec{u}_{23}$  and  $\vec{v}_{01} = \vec{v}_{23}$ .

The general SLP ansatz, Eq. (7), allows also other solutions that fulfill the length constraints. It is not the purpose here to find all solutions, but rather to describe a selected set that is most likely to be realized in finite-temperature systems.

The coplanar SLP<sub>1</sub> solution in Eq. (8) is a special case of a more general solution where the non-zero  $\vec{u}$ 's and  $\vec{v}$ 's are

$$\vec{u}_{01} = \vec{u}_{23}, \quad \vec{v}_{01} = \vec{v}_{23}, \quad \vec{v}_{02} = \vec{v}_{12} = \vec{v}_{03} = -\vec{v}_{13}, \quad (9)$$

with  $\vec{u}_{23}$  being a unit vector that is *perpendicular* to two other unit vectors  $\vec{w}_1$  and  $\vec{w}_2$  which parametrize

$$\vec{v}_{13} = (\vec{w}_1 + \vec{w}_2)/3, \quad \vec{v}_{23} = (2\vec{w}_1 - \vec{w}_2)/3.$$
 (10)

The presence of the other  $\vec{v}$ 's in addition to  $\vec{v}_{01}$  and  $\vec{v}_{23}$  causes the appearance of all momentum vectors  $\vec{Q}_{ij}$  in the spin configuration. Thus, this state is a  $6\vec{Q}$ -state when  $\vec{v}_{13} \neq 0$ . A general property of these states is that spins on sublattices 0 and 1 (2 and 3) with identical trisublattice and plane indices are antiparallel, and spins on sublattices 0 and 2 (1 and 3) with identical trisublattice and plane index are parallel. Additionally, the spins in one of the three planes on the same sublattice are in general different from the spins in the remaining

two planes. Thus, the strict up-down alternation along directions  $\vec{a}_0-\vec{a}_1$  and  $\vec{a}_2-\vec{a}_3$  does in general no longer hold

The special case  $\vec{w}_1 = -\vec{w}_2$  implies  $\vec{v}_{13} = 0$  and corresponds to the coplanar SLP<sub>1</sub> solution above, where the three planes on each sublattice are equal. For  $\vec{w}_1 = \vec{w}_2$ , we find a coplanar state that differs slightly from SLP<sub>1</sub>. In this state, two spins on one of the triangular planes on every sublattice is permuted, so that the chirality of the 120° arrangement in that plane is opposite to the remaining two planes.

For non-collinear arrangements of  $\vec{w}_1$  and  $\vec{w}_2$ , one gets a non-coplanar spin state. Because of the non-coplanarity, we expect this state to have smaller entropy than the coplanar SLP<sub>1</sub> state, and less likely to be realized at finite temperatures.

#### B. Finite field

In a finite magnetic field, the general zero-field solution Eqs. (9,10) gives unit length spins if  $\vec{u}_{23}$ ,  $\vec{w}_1$  and  $\vec{w}_2$  are modified to be vectors of length  $\sqrt{1-m^2}$  perpendicular to the field. This implies a configuration where the  $\perp$ components of the spins with identical trisublattice and plane indices are antiparallel on sublattices 0 and 1 (2) and 3) and parallel on sublattices 0 and 2 (1 and 3). The \( \| \)-components of all the spins are identical and equal to the magnetization per spin m. However, since the vectors  $\vec{u}_{23}$ ,  $\vec{w}_1$  and  $\vec{w}_2$  lie in the plane perpendicular to the magnetic field and  $\vec{u}_{23}$  must be perpendicular to both  $\vec{w}_1$  and  $\vec{w}_2$ , there are only two possibilities for  $\vec{w}_1$  and  $\vec{w}_2$ given  $\vec{u}_{23}$ . In the first case, the  $\vec{w}$ 's are antiparallel, giving a canted version of SLP<sub>1</sub>. This state is essentially SLP<sub>1</sub> within the  $\perp$ -plane, but with all spins having the same finite "-component (see Fig. 1). The other case, parallel  $\vec{w}$ 's, gives similarly a canted version of the zero-field state where one plane of spins has an opposite chirality inplane 120° arrangement than in the other two planes.

The previously discussed non-coplanar zero-field solutions have no analog in a magnetic field. However, there are other classes of solutions which resemble the previous ones in that any spin on a given sublattice is "antiparallel" to one spin on two of the sublattices (in a field we use the term "antiparallel" for two spins having opposite  $\perp$ -components and equal  $\parallel$ -components) and parallel to a spin on the remaining sublattice. Such solutions are more likely to have high entropy due to the high number of (anti)parallel spins. We have found one particularly interesting example of this, where spins that are "antiparallel" do no longer have equal plane indices, as was the case for the solutions discussed previously. Instead, the spins in planes (0,1,2) on sublattice 0 (2) are "antiparallel" to the spins of equal trisublattice index in

planes (0, 2, 1) on sublattice 1 (3), which leads to

$$\begin{split} u_{12}^{\perp} &= -u_{03}^{\perp}, \ u_{12}^{\parallel} = +u_{03}^{\parallel}, \\ v_{12}^{\perp} &= +v_{03}^{\perp}, \ v_{12}^{\parallel} = -v_{03}^{\parallel}, \\ u_{13}^{\perp} &= -u_{02}^{\perp}, \ u_{13}^{\parallel} = +u_{02}^{\parallel}, \\ v_{13}^{\perp} &= -v_{02}^{\perp}, \ v_{13}^{\parallel} = +v_{02}^{\parallel}, \\ u_{01}^{\parallel} &= 0, \ v_{01}^{\parallel} = 0, \ u_{23}^{\parallel} = 0, \ v_{23}^{\parallel} = 0. \end{split}$$

Furthermore the spins on sublattices 0 (1) and 2 (3) are parallel for equal plane indices, implying

$$\vec{u}_{02} = 0,$$
 $u_{03}^{\parallel} = 0, \quad v_{03}^{\parallel} = 0,$ 
 $\vec{u}_{23} = \vec{u}_{01}, \quad \vec{v}_{23} = \vec{v}_{01}.$ 

Even with these conditions, there are many solutions. However, solutions different from those already classified have  $\vec{v}_{02}^{\perp}=0$ . The normalization problem then reduces to nine equations (normalization of the nine spins on sublattice zero) with eleven unknowns. We solve these 9 equations, leaving the direction of  $\vec{u}_{01}$  and the angle  $\alpha-\pi/2$  between  $\vec{u}_{01}$  and  $\vec{u}_{03}$  as free parameters. We find that  $\vec{u}_{01}$  ( $\vec{u}_{03}$ ) and  $\vec{v}_{01}$  ( $\vec{v}_{03}$ ) must be orthogonal vectors of length  $\sqrt{a+b}$  ( $\sqrt{a-b}$ ), where

$$a = \frac{1}{2}(1 - m^2 - 8m^2 \tan^2 \alpha),$$
  
$$b = \frac{1}{2}\sqrt{(1 - m^2)^2 - 16m^2(1 + 3m^2)\tan^2 \alpha}.$$

Additionally, the directions of  $\vec{v}_{01}$  and  $\vec{v}_{03}$  must be chosen to satisfy

$$\vec{u}_{01} \cdot \vec{v}_{03} = \vec{u}_{03} \cdot \vec{v}_{01}.$$

The non-zero component of  $\vec{v}_{02}$  is  $v_{02}^{\parallel} = -4|\vec{m}|\tan \alpha$ . Lastly, the angle  $\alpha$  is restricted by

$$\alpha \in [0, \alpha_{max}] \cup [\pi - \alpha_{max}, \pi], \tag{11}$$

where

$$\tan \alpha_{max} = \frac{1 - m^2}{4|m|\sqrt{(1 + 3m^2)}}. (12)$$

For  $\alpha=\{0,\pi\}$ , this solution is the canted SLP<sub>1</sub> state with  $\vec{u}_{01}^2=1-m^2$  and  $\vec{u}_{03}^2=\vec{v}_{02}^2=0$ . As  $\alpha$  is increased (decreased) from 0  $(\pi)$ , the canted SLP<sub>1</sub> state continuously evolves into a state where each sublattice has three  $\vec{Q}$ s; SLP<sub>3, $\alpha$ </sub> (with six  $\vec{Q}$ s in total). In this state, there is a different order in each of the three triangular planes on a given sublattice. An explicit parametrization of this SLP<sub>3, $\alpha$ </sub> state is shown in Appendix B. The value  $\alpha_{max}$  gives the "maximal" SLP<sub>3, $\alpha$ </sub> state, where  $|\vec{u}_{01}|=|\vec{u}_{03}|$ . We will refer to this as the SLP<sub>3,M</sub> state (see Fig. 2).

In the SLP<sub>3, $\alpha$ </sub> states, the spin components along the magnetic field take three values:  $\{m, m(1 \pm 2\sqrt{3} \tan \alpha)\}$ .

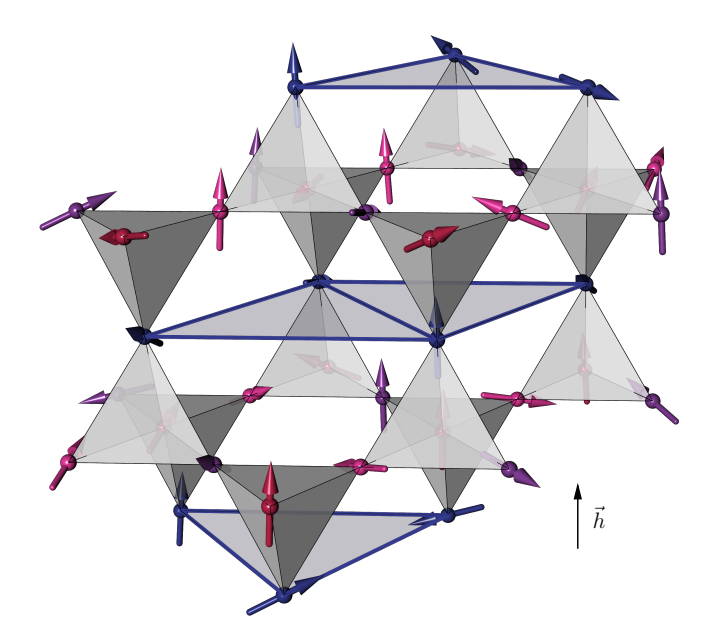


FIG. 2. The  $SLP_{3,M}$  state in magnetic field h=4. The spins have three different  $\parallel$ -components, and for each sublattice there are three different triangular plane spin configurations that repeats itself with period three.

This is a consequence of only  $\vec{v}_{02}$  having a finite  $\parallel$ -component. For  $\alpha = \{0, \pi\}$ , all spin  $\parallel$ -components become equal to m (canted SLP<sub>1</sub>). The difference in the three values along the field increases as  $\alpha$  approaches  $\alpha_{max}$ .

Taking the limit  $m \to 0$ , we note that  $\mathrm{SLP}_{3,\alpha}$  approaches the coplanar single- $\vec{Q}$   $\mathrm{SLP}_1$  state for all  $\alpha \neq \alpha_{max}$ , while for  $\alpha = \alpha_{max}$ , we instead get a non-coplanar zero-field analog of the  $\mathrm{SLP}_{3,M}$  state, different from the previously discussed zero-field solutions.

We note that other solutions similar to  $\mathrm{SLP}_{3,\alpha}$  can be found by transforming  $\vec{R}$  according to the lattice symmetries. This will lead to solutions with other pairings of "antiparallel" and parallel planes and trisublattice indices, depending on the transformation.

## IV. SPIN WAVE ENTROPY

For a given value of the magnetic field, all states described by the ansatz in Eq. (7) have equal energies. To determine which of these are favored at finite temperatures, we compute their entropy using linear spin wave theory. We assign each particular ground state to a periodic system with the unit cell of  $M=3^3\times 4=108$  spins on the fcc lattice. The spin configurations define site-dependent rotated frames, in terms of which the spins are in a ferromagnetic configuration. We then use the Holstein-Primakoff [30] transformation to describe the deviations from the ferromagnetic configuration as bosons. The resulting boson Hamiltonian is expanded

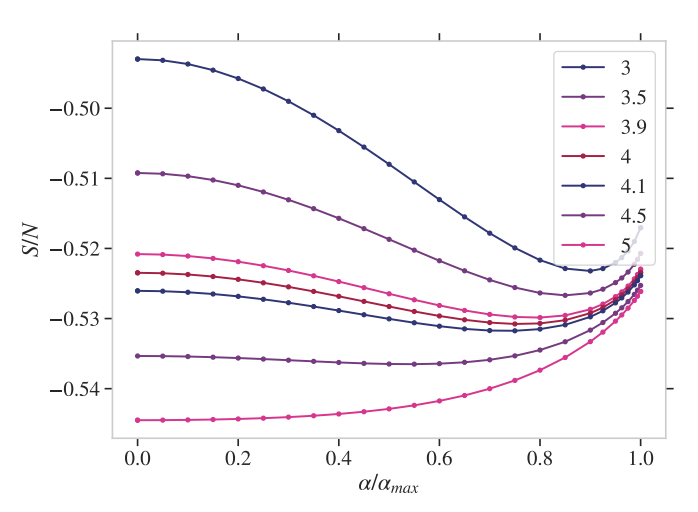


FIG. 3. Entropy per spin vs.  $\alpha$  for different values of the magnetic field.  $J_1 = 1, J_{3b} = 0.2$ .

to quadratic order, with vanishing linear terms. This Hamiltonian is then diagonalized numerically to obtain the spin wave frequencies  $\omega_{\vec{q},i}$ , using a Bogoliubov transformation involving 2M bosons [31]. For further details, see Appendix C.

The entropy per site from these linear spin wave fluctuations can then be computed as

$$S/N = -\frac{1}{l^3 M} \sum_{\vec{q}} \sum_{i=1}^{M} \ln \omega_{\vec{q},i},$$
 (13)

where the sum  $\vec{q}$  goes over the first Brillouin zone of the lattice with  $l^3$  M-site unit cells. In order to find the entropy for  $l \to \infty$ , we compute the entropy for sizes  $l = \{6, 9, 12, 15, 18\}$  and extrapolate S/N vs.  $1/l^3$  to infinite size using a quadratic polynomial.

For h = 0, we confirm that the spin wave entropy favors the coplanar  $SLP_1$  state (see Appendix D). For finite fields, we compute the entropy per site (for  $l \to \infty$ ) for  $SLP_{3,\alpha}$  as a function of  $\alpha$ , as shown in Fig. 3 for  $J_1=1$ and  $J_{3b} = 0.2$ . The Bogoliubov diagonalizations for these configurations yield four gapless modes, which are regularized by adding a small value  $10^{-10}$  to the diagonal of the Hamiltonian matrix. It is seen that for low fields (h < 4), the entropy is maximal for  $\alpha = 0$ , corresponding to the canted  $SLP_1$  state. For higher fields (h > 4), the entropy is instead maximal for  $\alpha = \alpha_{max}$ , corresponding to  $SLP_{3,M}$ . Fig. 3 also shows that the change between these two values (0 and  $\alpha_{max}$ ) at h=4 is discontinuous. To better see that the change happens at h = 4, we compare the values of the entropy per site vs. magnetic field for the two  $\alpha$  values in Fig. 4.

## V. ORDER PARAMETERS

To distinguish the SLP<sub>1</sub> state from the SLP<sub>3</sub> states in the subsequent numerics, we construct three order pa-

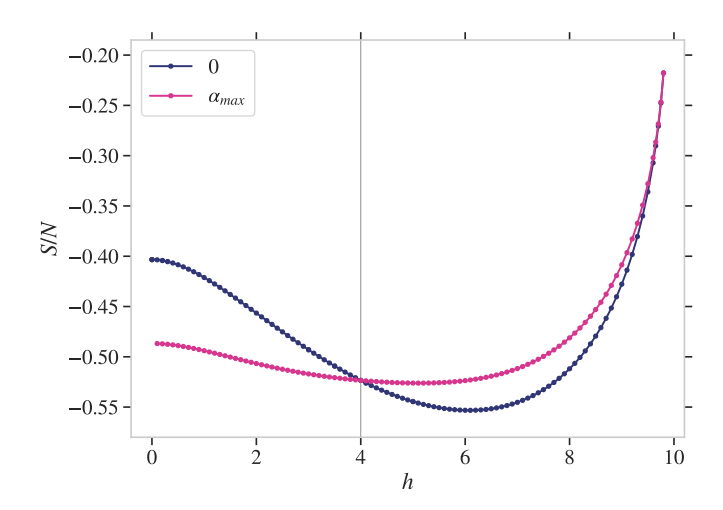


FIG. 4. Entropy vs. magnetic field for  $\alpha=0$  and  $\alpha=\alpha_{max}$ .  $J_1=1,\ J_{3b}=0.2.$ 

rameters. For the first order parameter, we make use of the fact that the  $SLP_1$  state can be viewed as two sets of crossing parallel chains where the spins on each chain are ordered in an "antiparallel" way. In an  $SLP_1$  state with (01)&(23) pairing, one set of chains runs along the direction  $\vec{a}_1 - \vec{a}_0$  involving alternate sublattice 0 and 1 sites. The other set runs along the direction  $\vec{a}_3 - \vec{a}_2$  and involves sites on the sublattices 2 and 3 (see Fig. 1). For one chain involving sublattices i and j, we define the chain staggered order parameter as

$$\vec{C}_{\vec{R}_{0},ij} \equiv \frac{1}{2L} \sum_{n} \left( \vec{S}_{\vec{R}_{0}+n(\vec{a}_{j}-\vec{a}_{i}),i} - \vec{S}_{\vec{R}_{0}+n(\vec{a}_{j}-\vec{a}_{i}),j} \right),$$
(14)

where  $\vec{R}_0$  is an arbitrary up tetrahedron on the chain. We take the average length of this over all chains, which is achieved by taking the average over all up tetrahedra in the lattice

$$C_{ij}^2 \equiv \frac{1}{L^3} \sum_{\vec{R}_0} \vec{C}_{\vec{R}_0, ij} \cdot \vec{C}_{\vec{R}_0, ij}. \tag{15}$$

From this, we construct the three-component complex SLP order parameter,  $O_{\rm SLP}$ , where each component corresponds to a particular way of pairing the sublattices,

$$O_{\text{SLP}} = C_{01}C_{23} + e^{i2\pi/3}C_{02}C_{13} + e^{i4\pi/3}C_{03}C_{12}. \quad (16)$$

In the MC simulations, we measure all the  $C_{ij}$ s and compute the modulus  $|O_{\text{SLP}}|$ . A non-zero value will be taken as an indicator of an SLP phase. In Appendix E it is shown that for a state respecting the SLP ansatz in Eq. (7),

$$C_{ij}^2 = \frac{1}{2} \left( \vec{u}_{ij}^2 + \vec{v}_{ij}^2 \right) \tag{17}$$

and

$$|O_{\rm SLP}| = \sqrt{(1 - \vec{m}^2)^2 - 3(C_{01}^2 C_{02}^2 + C_{01}^2 C_{03}^2 + C_{02}^2 C_{03}^2)}.$$
(18)

The maximum value occurs for the canted  $SLP_1$  state, where only one of  $C_{01}$ ,  $C_{02}$  and  $C_{03}$  is non-zero, giving

$$|O_{\text{SLP},1}| = 1 - m^2. \tag{19}$$

In the  $SLP_{3,M}$  state, we get

$$|O_{\text{SLP},M}| = \left| \frac{(1-m^2)(1-9m^2)}{4(1+3m^2)} \right|.$$
 (20)

Another property of the canted  $SLP_1$  state is that all spin  $\parallel$ -components are equal. To detect deviations from this, we calculate the spatial fluctuations of the magnetization in the field-direction

$$\kappa \equiv \frac{1}{N} \sum_{\vec{r}} \left( S_{\vec{r}}^{\parallel} - m \right)^2. \tag{21}$$

For the canted SLP<sub>1</sub> state;  $\kappa = 0$ , while for the SLP<sub>3,M</sub> state

$$\kappa_M = \frac{(1 - m^2)^2}{2(1 + 3m^2)}. (22)$$

Lastly,  $SLP_1$  and  $SLP_3$  can be distinguished by only  $SLP_3$  having a non-vanishing tetrahedral scalar chirality [23, 32]

$$O_{\chi} = \frac{4}{N} \sum_{\vec{R}} \chi(\vec{R}), \tag{23}$$

where  $\chi(\vec{R})$  is the sum of the chiralities for the four faces of the up tetrahedron at  $\vec{R}$ . The chirality of a face is computed such that its three spins are ordered in a counter-clockwise direction w.r.t. the outward face normal:

$$\chi(\vec{R}) = \vec{S}_{\vec{R},1} \cdot (\vec{S}_{\vec{R},2} \times \vec{S}_{\vec{R},3}) + \vec{S}_{\vec{R},3} \cdot (\vec{S}_{\vec{R},0} \times \vec{S}_{\vec{R},1}) + \vec{S}_{\vec{R},0} \cdot (\vec{S}_{\vec{R},3} \times \vec{S}_{\vec{R},2}) + \vec{S}_{\vec{R},2} \cdot (\vec{S}_{\vec{R},1} \times \vec{S}_{\vec{R},0}).$$
(24)

For the  $\mathrm{SLP}_{3,\alpha}$  state,  $O_{\chi} = 2 \left(4m \tan \alpha\right)^3$ , which means that it is zero for the canted  $\mathrm{SLP}_1$  state  $(\alpha = 0)$  and

$$O_{\chi,M} = 2\left(\frac{1-m^2}{\sqrt{1+3m^2}}\right)^3$$
 (25)

for  $SLP_{3,M}$ .

#### VI. NUMERICAL RESULTS

To get an independent confirmation of our analytical results, we have performed classical MC simulations on systems with an fcc lattice of tetrahedra with periodic boundary conditions. The simulations were carried out using single-spin Metropolis moves [33], where each spin is selected as a random vector in spin space [34]. As the acceptance ratio of these Metropolis updates were only a few percent at the lowest temperatures, we included also other types of MC updates: Over-relaxation

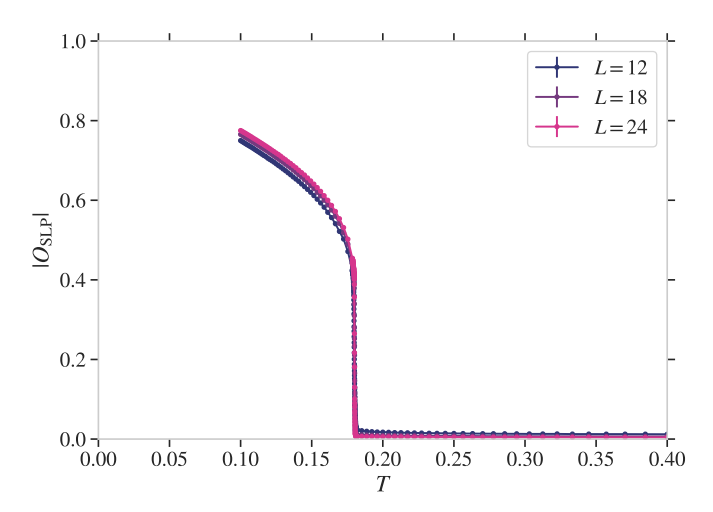


FIG. 5. Parallel tempering Monte Carlo results for the SLP order parameter vs. temperature in zero magnetic field.

moves [34] where the spin is rotated an arbitrary angle about the effective magnetic field axis seen on each site, a Wolff-cluster update [35] where clusters are formed of spins that will be mirrored on an arbitrary plane that includes the magnetic field direction (so that  $S^{\parallel}$  does not change), single-spin Metropolis moves where a specific spin component on each spin is attempted flipped, and a single-spin Metropolis move where the proposed change is restricted to lie in a cone about the old spin [34, 36, 37]. In some of the simulations, we also implemented the parallel tempering setup [38] with a feedback-optimized scheme [39] to select a set of temperatures that cause as many round-trips as possible for each replica. The parallel tempering simulations were run with a fixed number of typically 20-50 replicas spanning a fixed temperature interval, with more replicas if the system is large in order to increase the replica swapping rate. In the following we will show results for the parameter values  $J_1 = 1$  and  $J_{3b} = 0.2.$ 

All our low-temperature numerical simulations show results consistent with the magnetization relation Eq. (3) and ground state energy Eq. (4), confirming the form of the Hamiltonian in Eq. (2).

In Fig. 5, we show parallel tempering MC results for  $|O_{\rm SLP}|$  vs. temperature T in zero magnetic field for three different linear system sizes L ( $N=4L^3$ ). The SLP order parameter shows a steep increase at  $T_c=0.180$ , which is 8% lower than estimated using Nematic Bond Theory [8]. The system size dependence of the critical temperature is weak, and the rise of the order parameter resembles that of a discontinuous phase transition, in accordance with the Nematic Bond Theory results. When extrapolating to zero temperature, the SLP order parameter appears to reach the value 1, consistent with the low-temperature phase being the SLP<sub>1</sub> state (with thermal fluctuations).

When a magnetic field is added, the MC simulations are in general more difficult to equilibrate, thus we were forced to use smaller system sizes. Using a system size

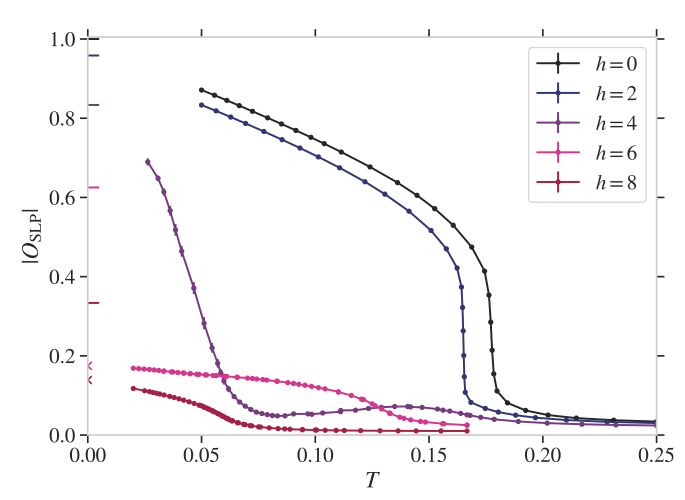


FIG. 6. Parallel tempering Monte Carlo results for the SLP order parameter vs. temperature for different values of the magnetic field indicated in the legend. L=6. The short horizontal colored bars on the ordinate axis indicate the SLP<sub>1</sub> values of the SLP order parameter;  $1-m^2$ . The colored crosses on the ordinate axis indicate the SLP<sub>3,M</sub> values of the SLP order parameter from Eq. (20).

of L=6, we show in Fig. 6 the SLP order parameter vs. temperature for different values of the magnetic field. The sharp rise of the SLP order parameter that was seen for zero field is still present for fields  $h\lesssim 4.5$ , and it appears to extrapolate to a value close to  $1-m^2$  as  $T\to 0$ , shown as colored horizontal bars on the ordinate axis. This is consistent with the low-temperature phase being the canted SLP<sub>1</sub> state. The associated critical temperature decreases as the magnetic field is increased.

We also observe from Fig. 6 that for small fields,  $h \leq 2$ , the system goes directly from the high-temperature disordered phase into the canted SLP<sub>1</sub> phase at low temperatures. In contrast, for  $2 \lesssim h \lesssim 4.5$  coming from high temperatures, there is first a slight increase in the SLP order parameter before it slightly decreases, and then increases sharply at a lower temperature (see the h=4curve in Fig. 6). For  $h \gtrsim 4.5$  we find only the slight increase in the SLP order parameter, and no dramatic upturn down to the lowest temperatures studied (T > 0.02). Instead, the SLP order parameter extrapolates to a value close to that for the  $SLP_{3,M}$  state when T goes to zero, shown as crosses on the ordinate axis. We thus interpret the slight increase of the SLP order parameter as entering the  $SLP_{3,M}$  phase and the more pronounced increase as entering the SLP<sub>1</sub> phase. To preliminary summarize these data, we draw in Fig. 7 an outline of the phase diagram, which will be further substantiated below.

To verify the  $SLP_{3,M}$  part of the phase diagram at low temperatures, we have carried out long standard MC simulations without parallel tempering, all started from the canted  $SLP_1$  state. They were run for  $10^9$  MC steps, each at a fixed temperature. In Fig. 8, we show the spatial magnetization fluctuations  $\kappa$  (scaled by the expected value  $\kappa_M$  in the  $SLP_{3,M}$  state) for ten independent sim-

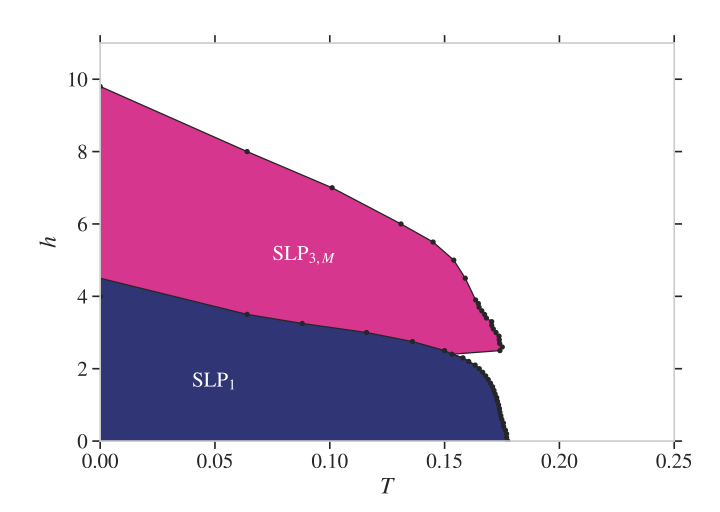


FIG. 7. Outline of the phase diagram indicating the phase transition (solid line) from the high-temperature phase into the  $SLP_1$  (blue) and  $SLP_{3,M}$  (pink) phases. L=6.

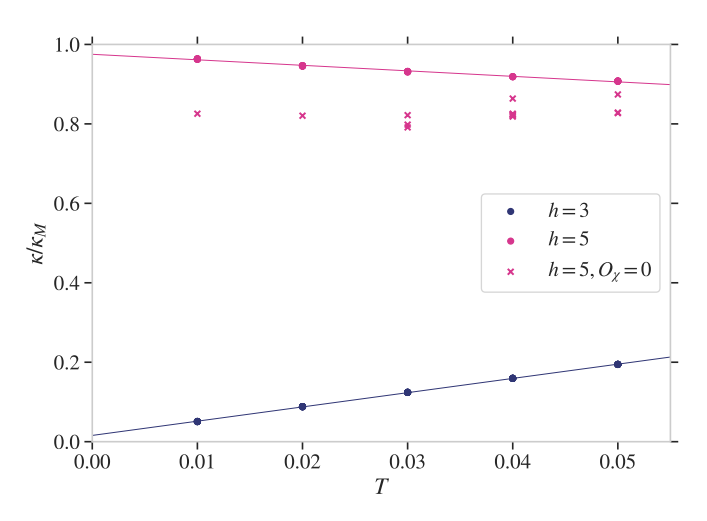


FIG. 8. Scaled magnetization fluctuations  $\kappa$  at low temperatures for magnetic fields h=3 and 5. L=6. Many points are on top of each other as we show the results for ten independent runs for each temperature and field value.

ulations at each temperature and field value. It is apparent that for h=5, all simulations have escaped the initial  $\mathrm{SLP}_1$  state. Most of them (circles) get a value for  $\kappa$  which comes very close to the  $\mathrm{SLP}_{3,M}$  value when  $T\to 0$ . There are also runs with slightly smaller values of  $\kappa$  (crosses), that are further distinguished from the others (circles) by having at least an order of magnitude smaller chirality  $|O_{\gamma}|$ .

Taking the final spin configurations of these runs, and exposing them to an energy relaxation procedure, we relax the spin configurations to the corresponding ground state (relaxed energies differ from Eq. (4) by at most  $10^{-12}$ ). We find that the spin configurations corresponding to higher  $\kappa$  relax to  $SLP_{3,M}$ , while the ones with smaller  $\kappa$  attain a more complicated non-coplanar zero chirality configuration that satisfies the ansatz Eq. (7),

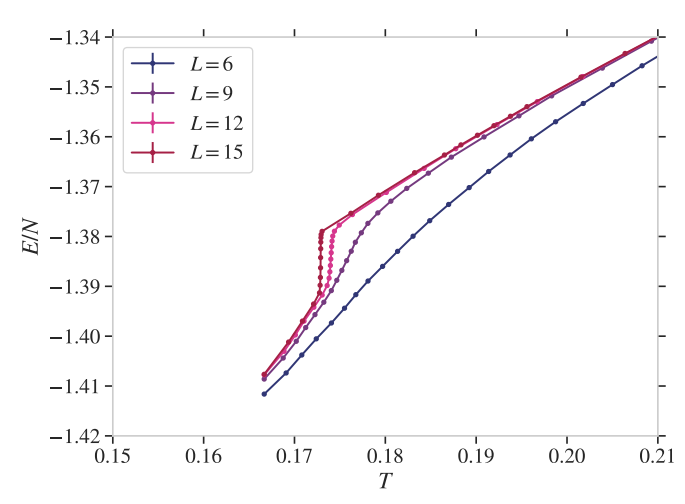


FIG. 9. Energy per site vs. temperature around the high-temperature phase transition for h=2.5 for different system sizes.

but which is not among the solutions outlined in Sec. III. While the chirality on individual up tetrahedra are generally non-zero in this state, their sum is zero. We have calculated the entropy per site of this zero chirality state to be -0.53056, which is lower than the value -0.526129 obtained for  $\mathrm{SLP}_{3,M}$  (h=5). Thus, we expect that finite temperature entropy selection will eventually prefer the  $\mathrm{SLP}_{3,M}$  state for even longer MC runs.

For h = 3,  $\kappa$  goes to zero as  $T \to 0$  for all runs. This is consistent with  $SLP_1$ , which is also what the energy relaxation procedure on these states shows.

The phase transition into the SLP<sub>1</sub> state at zero and small magnetic fields is discontinuous. This is also the case for the transition into the  $SLP_{3,M}$  phase, as shown in Fig. 9, where we show the energy per site at h=2.5vs. temperature for different system sizes. At  $T \simeq 0.175$ the curves develop with system size into a "knee" discontinuity, indicating a first order phase transition. This is however not the same temperature at which the SLP<sub>1</sub> order parameter increases dramatically, which happens at a lower temperature, where the energy per site shows a further drop with temperature, see Fig. 10. The resulting specific heat vs. temperature then exhibits two peaks as seen in the inset of Fig. 10. The magnitude of the highest temperature peaks associated with the discontinuous transition into the SLP<sub>3</sub> phase clearly increase with increasing system size, consistent with the development of the "knee" discontinuity in Fig. 9. The positions of the specific heat peaks associated with the steep rise of the SLP order parameter at lower temperatures depend on the system size, but their magnitudes do not.

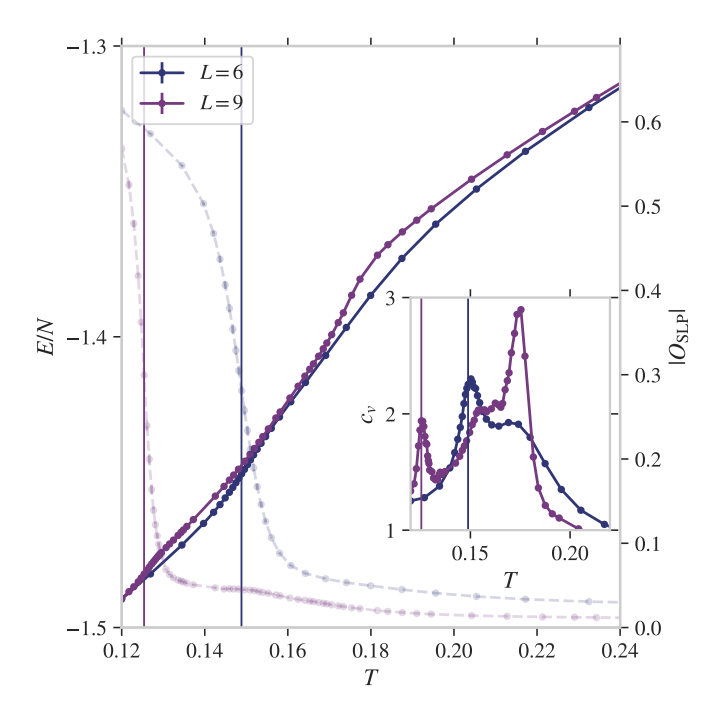


FIG. 10. Energy per site (solid lines) and the SLP order parameter (faint dashed lines) vs. T for h=2.5 for two different system sizes. The inset shows the corresponding specific heat. The vertical lines show the lowest peak temperatures of the specific heat.

## VII. STATIC STRUCTURE FACTORS

The ordered SLP states cause Bragg peaks in the static structure factors

$$S^{\mu\nu}(\vec{q}) \equiv \frac{1}{2} \left( S^{\mu}_{-\vec{q}} S^{\nu}_{\vec{q}} + S^{\nu}_{-\vec{q}} S^{\mu}_{\vec{q}} \right), \tag{26}$$

which can be measured in neutron scattering experiments.  $S_{\vec{q}}^{\mu}$  is the Fourier transform of the spin  $\mu$ -components in the ground state. For the SLP ansatz, Eq. (7), the longitudinal structure factor (taking  $\vec{h}$  along the z-axis) becomes

$$S^{zz}(\vec{q}) = \frac{N^2}{32} \sum_{\vec{G}} \left\{ \sum_{i < j} \left( u_{ij}^{z2} + v_{ij}^{z2} \right) \Theta \left[ \vec{G} \cdot (\vec{a}_i - \vec{a}_j) \right] \right. \\ \times \left( \delta_{\vec{q}, \vec{G} + \vec{Q}_{ij}} + \delta_{\vec{q}, -\vec{G} - \vec{Q}_{ij}} \right)$$

$$\left. + 2m^{z2} \left| 1 + e^{i\vec{G} \cdot \vec{a}_1/2} + e^{i\vec{G} \cdot \vec{a}_2/2} + e^{i\vec{G} \cdot \vec{a}_3/2} \right|^2 \delta_{\vec{q}, \vec{G}} \right\},$$
(27)

where  $\Theta[\vec{G}\cdot(\vec{a}_i-\vec{a}_j)]\equiv 1-\cos{(\pi(k_i-k_j))},\,\vec{G}=k_1\vec{b}_1+k_2\vec{b}_2+k_3\vec{b}_3$  denotes reciprocal lattice vectors of the fcc Bravais lattice, and  $k_0=0$ . The transversal structure factors are similar, but with x (or y)-components instead of z and no m-term.

These structure factors have non-trivial peaks outside of the first Brillouin zone for  $\vec{q} = \vec{Q}_{ij} + \vec{G}$  only when

 $k_i - k_j$  is odd. The peak intensities are

$$S^{\mu\nu}(\pm \vec{Q}_{ij} + \vec{G}) = \left(\frac{N}{4}\right)^2 \left(u^{\mu}_{ij}u^{\nu}_{ij} + v^{\mu}_{ij}v^{\nu}_{ij}\right), \quad k_i - k_j \in \text{odd.}$$
(28)

The longitudinal structure factor has an additional peak in the first Brillouin zone; at  $\vec{q} = 0$  with magnitude  $(Nm)^2$ , reflecting the total magnetization squared.

#### VIII. DYNAMICAL STRUCTURE FACTORS

From the linear spin waves calculation outlined in Sec. IV and Appendix C, we compute the zero-temperature dynamical structure factor

$$S^{\mu\nu}(\vec{q},\omega) = \int_{-\infty}^{\infty} dt \sum_{\vec{r},\vec{r}'} \langle S^{\mu}_{\vec{r}}(t) S^{\nu}_{\vec{r}'}(0) \rangle e^{-i\vec{q}\cdot(\vec{r}-\vec{r}')} e^{i\omega t}.$$
(29)

To make plots of this, we approximate the delta-functions coming from the spin wave calculation by Gaussians centered on the excitation frequency with a standard deviation 0.01, and plot the resulting intensity along straight lines in momentum space going from  $-\mathbf{K}_{ij}$  thru the zone center  $\Gamma$  to  $\mathbf{K}_{ij} = 9\vec{Q}_{ij}/8$ . To make the discussion of locations in momentum space precise, we define sets of momenta

$$\bar{Q}_{ij} \equiv \{\vec{Q}_{ij} + k_1 \vec{b}_1 + k_2 \vec{b}_2 + k_3 \vec{b}_3\}, \ \forall \ k_i - k_j \in \text{odd.}$$
 (30)

We will refer to  $S^{zz}(\vec{q},\omega)$  and  $(S^{xx}(\vec{q},\omega)+S^{yy}(\vec{q},\omega))/2$  as the longitudinal and transverse dynamical structure factors, respectively. The dynamical structure factors are in general rather complex because of the large 108-site unit cell, so we focus the discussion on the lowest energy modes.

In Fig. 11, we show the transverse and longitudinal dynamical structure factors in the Brillouin zone centered at  $\vec{b}_1 + \vec{b}_2 + \vec{b}_3$  for the SLP<sub>1</sub> state in zero magnetic field, Eq. (8), where  $\vec{u}_{01} = \vec{u}_{23}$  and  $\vec{v}_{01} = \vec{v}_{23}$  are chosen to lie in the xy-plane. There are in total 14 different gapless modes. Two of these are associated with the transverse channel at  $\bar{Q}_{01}$  and  $\bar{Q}_{23}$ . They connect to the Bragg peaks at the same locations caused by the explicit appearance of  $Q_{01}$  and  $Q_{23}$  in the ground state configuration. The remaining twelve gapless modes are visible only in the longitudinal structure factor. They appear at all  $Q_{ij}$ s, although there are no associated longitudinal Bragg peaks. Four of these have spectral weights at  $\pm \bar{Q}_{01}$  and  $\pm \bar{Q}_{23}$ , four at  $\pm \bar{Q}_{02}$  and  $\pm \bar{Q}_{13}$  and the remaining four at  $\pm \bar{Q}_{03}$  and  $\pm \bar{Q}_{12}$ . Slightly away from each  $\bar{Q}$ , however, there are at most two distinct highintensity low-energy spin wave branches, dependent on the directions in momentum space. We list the numbers for selected directions D in Table III.

The 14 gapless modes can be explained by linearizing the length constraint equations in small deviations  $\delta \vec{u}_{ij}$ 

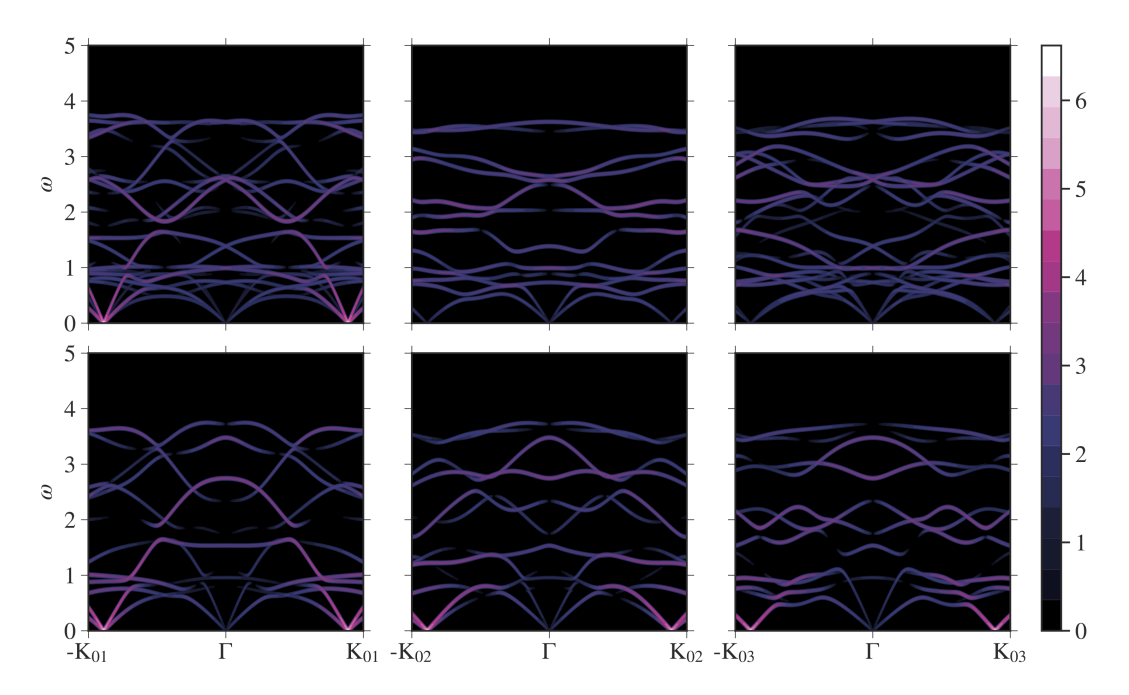


FIG. 11. Dynamical structure factor for the coplanar SLP<sub>1</sub> state in zero magnetic field in the Brillouin zone centered at  $\vec{b}_1 + \vec{b}_2 + \vec{b}_3$ . Upper (lower) panels show the transversal (longitudinal) channel. The colorbar shows  $\log[S(\vec{q},\omega)]$  with a cutoff for  $S(\vec{q}, \omega) < 1$ .

TABLE III. The number of longitudinal high-intensity lowenergy spin wave branches emanating out from  $\bar{Q}_{ij}$  in the direction  $\hat{D}$  when the ground state is SLP<sub>1</sub> with  $\vec{u}_{01} = \vec{u}_{23} = \hat{x}$ and  $\vec{v}_{01} = \vec{v}_{23} = \hat{y}$ . h = 0. n-fold degenerate branches are denoted:  $\times n$ . \* refers to the directions and  $\bar{Q}$ s shown in Fig. 11.

$\hat{D}$	$(\pm \bar{Q}_{01}, \pm \bar{Q}_{23})$	$(\pm \bar{Q}_{02}, \pm \bar{Q}_{13})$	$(\pm \bar{Q}_{03}, \pm \bar{Q}_{12})$
$\hat{K}_{01},\hat{K}_{23}$	2*	$2 \times 2$	$1 \times 2$
$\hat{K}_{02},\hat{K}_{13}$	$2 \times 2$	$2^*$	$1 \times 2$
$\hat{K}_{03},\hat{K}_{12}$	2	2	1*
$\hat{X}_1$	$2 \times 2$	2	$1 \times 2$
$\hat{X}_2$	2	$2 \times 2$	$2 \times 2$
$\hat{X}_3$	$2 \times 2$	$2 \times 2$	$1 \times 4$
$\hat{L}_0, \hat{L}_1, \hat{L}_2, \hat{L}_3$	2	2	1
generic	2	2	1

and  $\delta \vec{v}_{ij}$  from the planar SLP<sub>1</sub> state. There are in total 36 independent  $\delta \vec{u}_{ij}$ - and  $\delta \vec{v}_{ij}$ -components. In zero field, the linearized equations reduce to 22 constraints, leaving us with 36-22=14 gapless modes. The constraints require all  $\perp$ -components to be zero except for  $\delta u_{01}^y = -\delta v_{01}^x$ and  $\delta u_{23}^y = -\delta v_{23}^x$ . The two different transverse modes are therefore caused by the relative phase between the oscillations of the unpaired sublattices (e.g. 0 and 2) being either zero or  $\pi$  ("scissor" mode), where the latter has the lowest energy. The remaining twelve modes are associated with modulations in the z-direction associated with each of the twelve  $u_{ij}^z$ 's and  $v_{ij}^z$ 's.

When including small magnetic fields, the SLP<sub>1</sub> ground state cants. In Fig. 12, we show the dynamical structure factor for such a canted SLP<sub>1</sub> state when h = 1. There are four gapless modes. Two of these are visible as two low-energy spin wave branches near  $Q_{01}$  and  $Q_{23}$ in the transverse channel, as discussed for zero field. The remaining two modes have strong intensities both at  $Q_{02}$ and  $Q_{13}$  in the longitudinal channel, and also at  $Q_{03}$  and  $\bar{Q}_{12}$  in the transverse channel. Although there are two gapless modes at these momenta, we find that only one distinct band of low-energy excitations emanate out of them; depending on the direction, either only one mode is visible, or the two are degenerate. The four gapless modes can be explained by the four independent ways of deforming the canted SLP<sub>1</sub> state to linear order without energy cost, as described by the linearized length constraint equations around the canted SLP<sub>1</sub> solution:

$$\delta u_{01}^y = -\delta v_{01}^x,\tag{31}$$

$$\delta u_{23}^y = -\delta v_{23}^x, (32)$$

$$\delta u_{03}^{x} = -\delta v_{03}^{y} = \delta u_{12}^{x} = \delta v_{12}^{y} = \tilde{m} \delta u_{13}^{z} = -\tilde{m} \delta u_{02}^{z}, \quad (33)$$
  
$$\delta u_{03}^{y} = \delta v_{03}^{x} = -\delta u_{12}^{y} = \delta v_{12}^{x} = \tilde{m} \delta v_{13}^{z} = \tilde{m} \delta v_{02}^{z}, \quad (34)$$

$$\delta u_{03}^y = \delta v_{03}^x = -\delta u_{12}^y = \delta v_{12}^x = \tilde{m} \delta v_{13}^z = \tilde{m} \delta v_{02}^z,$$
 (34)

where  $\tilde{m} \equiv m/\sqrt{1-m^2}$ , and all other components  $\delta \vec{u}_{ij}, \delta \vec{v}_{ij}$  are zero. In particular, the two last equations imply relations between the z-components of  $\delta \vec{u}_{02}$  and  $\delta \vec{v}_{02}$  and the *xy*-components of  $\delta \vec{u}_{03}$  and  $\delta \vec{v}_{03}$ , explaining why the gapless modes at  $\bar{Q}_{02}$  and  $\bar{Q}_{13}$  in the longitudinal channel also show up in the transverse channel at  $Q_{03}$  and  $Q_{12}$ .

For high magnetic field (h = 5) we calculate the

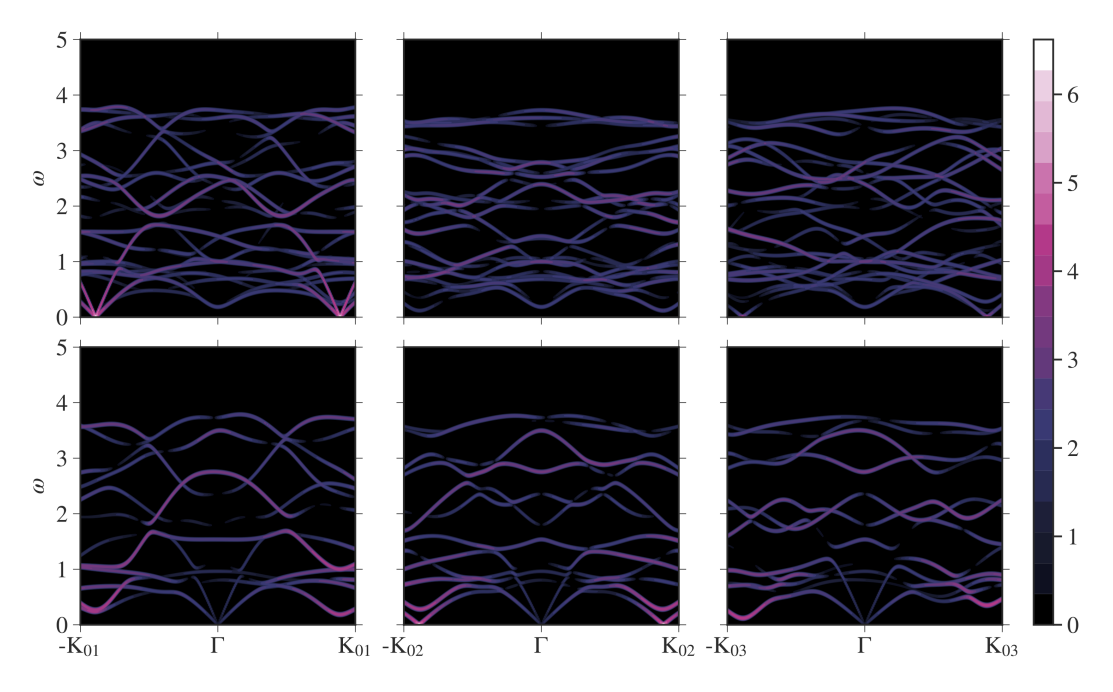


FIG. 12. Dynamical structure factor in the transversal (top) and longitudinal (bottom) channels for the canted SLP<sub>1</sub> state with (0,1) and (2,3) pairing in a magnetic field h=1 in the Brillouin zone centered at  $\vec{b}_1 + \vec{b}_2 + \vec{b}_3$ . The colorbar shows  $\log[S(\vec{q},\omega)]$  with a cutoff for  $S(\vec{q},\omega) < 1$ .

dynamical structure factor for the  $SLP_{3,M}$  state, see Fig. 13. It has more low-intensity spin wave branches than  $SLP_1$ . We find four gapless modes that are all dominantly transversal and each one has spectral weights on eight of the twelve different  $\pm Q_{ij}$ ; two of the modes lack spectral weights on  $\{\pm \bar{Q}_{02}, \pm \bar{Q}_{13}\}$ , the third on  $\{\bar{Q}_{03}, -\bar{Q}_{01}, -\bar{Q}_{12}, -\bar{Q}_{23}\}$ , and the fourth on  $\{-\bar{Q}_{03}, \bar{Q}_{01}, \bar{Q}_{12}, \bar{Q}_{23}\}$ . Therefore there are at most two low-energy transversal spin wave branches emanating out of  $\pm \bar{Q}_{02}$  and  $\pm \bar{Q}_{13}$ , and at most three for the other  $\bar{Q}_{ij}$ s. Linearizing the constraint equations around the  ${\rm SLP}_{3,M}$ state, we find that all  $\delta u_{ij}^z = \delta v_{ij}^z = 0$ , which explains why the gapless modes lack spectral weight in the longitudinal channel. Furthermore the linearized equations give  $\delta u_{02}^{\perp} = \delta u_{13}^{\perp} = 0$ , and conditions where the in-plane components  $\delta u_{ij}^{\perp}$  and  $\delta v_{ij}^{\perp}$  with  $ij = \{01, 03, 12, 13, 23\}$ are parametrized by the four independent components of  $\delta v_{02}^{\perp}$  and  $\delta v_{03}^{\perp}$ . In particular,  $\delta v_{13}^{\perp}$  only depends on the two components of  $\delta v_{02}^{\perp}$ . From this, it follows that there are only two gapless modes at  $\pm Q_{02}$  and  $\pm Q_{13}$ .

## IX. DISCUSSION

In Ref. 8, SLP<sub>1</sub> states were found to be the ground states of the classical pyrochlore Heisenberg antiferromagnet in zero magnetic field for an extended range of further-neighbor exchange interactions (with modified ordering wave vectors  $\vec{Q}_{ij}$ s). In these states, spins on pairs of sublattices form antiparallel coplanar spirals, and the ordering wave vectors for the two pairs are in general dif-

ferent. Here, we have found exact ground states for the pure AF  $J_1$ - $J_{3b}$  model in a magnetic field that generalize these  $\mathrm{SLP}_1$  states.

Our key finding is that the ground states can be described by the SLP ansatz in Eq. (7). This ansatz ensures a spin sum of  $4\vec{m}$  on every tetrahedron of  $J_1$  bonds, and  $3\vec{m}$  on every elementary triangle of  $J_{3b}$  bonds. It therefore describes ground states for all AF couplings  $J_1, J_{3b} > 0$ . In the limits where either  $J_{3b} = 0$  or  $J_1 = 0$ , the SLP ansatz is however too restrictive as then only the tetrahedron condition or the triangle condition, respectively, should hold. For  $J_{3b} = 0$ , i.e. the pure  $J_1$  model on the pyrochlore lattice in a magnetic field, the ground states constitute instead an extensive manifold with one degree of freedom per tetrahedron, i.e. N/2 degrees of freedom in total [28]. In the opposite limit of  $J_1 = 0$ , the system reduces to decoupled triangular planes in a magnetic field for which the triangle condition should hold [29, 40]. This leaves three degrees of freedom for each triangular plane. Computations of the spin wave entropy shows that the AF XY model on the triangular lattice in a magnetic field favors the coplanar Y and V states [41], and MC simulations have shown that the corresponding Heisenberg model orders in the same phases at finite temperature [29, 42, 43]. The case studied here, where both  $J_1$  and  $J_{3b}$  are non-zero, picks out the states which the two ground state manifolds have in common.

Our SLP ansatz generally describes spatially periodic multi- $\vec{Q}$  states with a large unit cell where the spins on pairs of sublattices have a tendency to be antiparallel in the plane perpendicular to the magnetic field and parallel

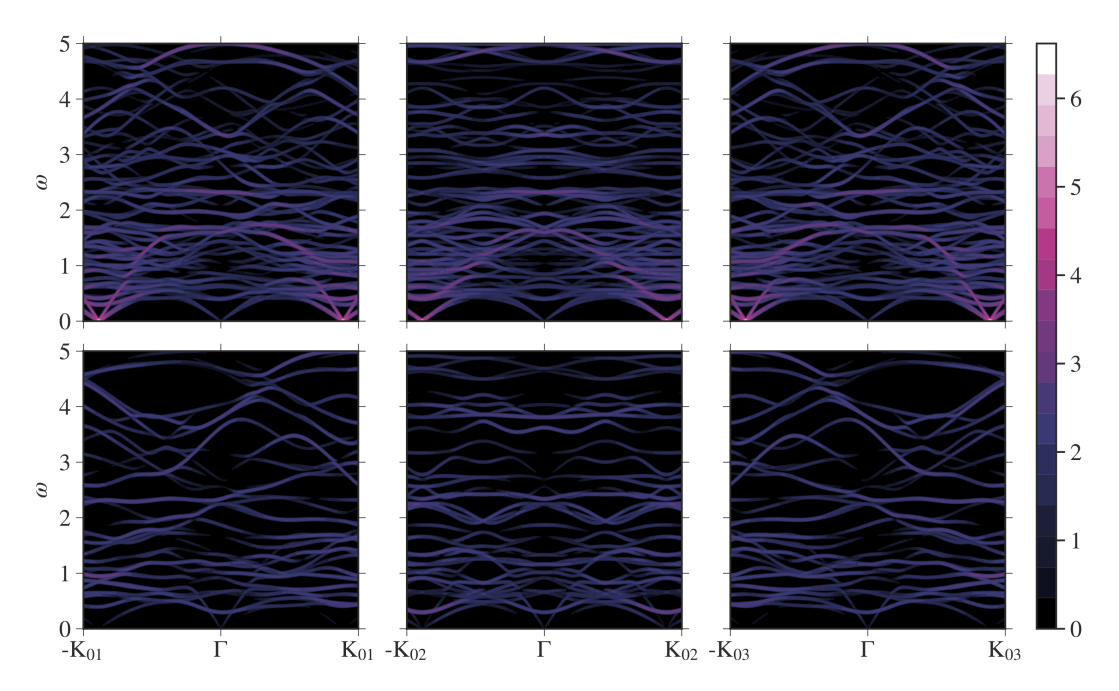


FIG. 13. Dynamical structure factor in the transversal (top) and longitudinal (bottom) channels for the  $SLP_{3,M}$  state in a magnetic field h=5 in the Brillouin zone centered at  $\vec{b}_1 + \vec{b}_2 + \vec{b}_3$ . The colorbar shows  $\log[S(\vec{q},\omega)]$  with a cutoff for  $S(\vec{q},\omega) < 1$ .

along the field. However, the ansatz itself is incomplete as one also need to choose its parameters such that all spins have unit length. Multi- $\vec{Q}$  states are typically incompatible with the unit length constraint. Nevertheless, we have here presented several normalized solutions. The simplest of these are the SLP<sub>1</sub> states, that are identical to those found in Ref. 8 in zero magnetic field. In a finite magnetic field the coplanar SLP<sub>1</sub> state smoothly goes into a canted SLP<sub>1</sub> state that develops a uniform spin component along the magnetic field and stays almost unchanged in the plane perpendicular to the field. This  $SLP_1$  state is a  $2\vec{Q}$ -state. The SLP ansatz harbors also  $6\vec{Q}$ -states, but no normalizable  $4\vec{Q}$ -states (see Appendix F). Most interestingly, we have parametrized a family of states that interpolates continuously from the canted  $SLP_1$  state into  $6\vec{Q}$   $SLP_3$  states, while keeping the spins normalized.

Finite temperatures induce an order-by-disorder mechanism favoring the state with the largest entropy. Using linear spin waves, we have calculated the entropy of the continuous family of SLP states. We find that for  $J_1 = 1, J_{3b} = 0.2$ , the canted SLP<sub>1</sub> state is favored for magnetic fields h < 4, while the  $6\vec{Q}$ -state SLP<sub>3,M</sub> has the highest entropy for h > 4. The MC simulations indicate a slightly larger value for the zero-temperature critical field of this phase transition:  $h_C \simeq 4.5$ . The slight discrepancy with linear spin wave theory is likely to be a consequence of the relatively small systems studied, but could also indicate a quantitative inadequacy of the linear spin wave approximation.

From the MC simulations, we conclude that the finite

temperature disordering of the  $SLP_1$  and  $SLP_{3,M}$  phases are both discontinuous. In addition, they indicate a magnetic field region (approximately  $h \in [2.5, 4.5]$ ) where the system first goes into the  $SLP_{3,M}$  phase and then into the  $SLP_1$  phase as the temperature is lowered in a fixed magnetic field. Lowering the field at a fixed temperature results in two phase transitions, and even an intermediate disordered phase for the highest temperatures, see Fig. 7. However, as evidenced by the system size dependence shown in Fig. 10, we expect the quantitative details of the phasediagram to change somewhat for larger system sizes.

The ordered SLP states should exhibit Bragg peaks in neutron scattering experiments. We have calculated the static structure factors and find Bragg peaks at momenta corresponding to the ordering wave vectors in specific Brillouin zones. The discrimination between the  $\mathrm{SLP}_1$  and  $\mathrm{SLP}_{3,M}$  phases can then be made based on whether neutron scattering shows two or six inequivalent Bragg-peaks at low temperatures in a single-domain single-crystalline material.

We have also computed the spin wave spectra of the SLP states and their corresponding dynamical structure factors. As is to be expected from a spin configuration with a large unit cell, the dynamical structure factor is rather complicated, having many spin wave branches with different intensities. Focusing on the lowest energies, the dynamical structure factors reveal gapless modes at all momenta where there is a corresponding Bragg peak in the static structure factor. This is the usual scenario where the low energy spin waves describe long wavelength deformations of a spin configuration around

its ordering wave vector. However, we also find additional high intensity gapless modes at momenta where there are no Bragg peaks.

In zero magnetic field, we find that the SLP<sub>1</sub> state has in total 14 different gapless modes. This is many more than guaranteed by the Goldstone theorem, where the completely broken continuous O(3) symmetry at h=0leads to three gapless modes. Our results are however not in conflict with the Goldstone theorem, as it only gives a lower limit on the number of gapless modes. In fact, the number of gapless modes seen in the linear spin wave calculation is in agreement with the number of independent solutions of the linearized spin normalization equations applied to the SLP ansatz. This indicates that the SLP ansatz is capable of describing all ground states in the vicinity of the SLP<sub>1</sub> state. One can speculate about the fate of the 14 gapless modes when doing a higher order spin wave calculation. As only three are protected by symmetry, many of them will probably become gapped.

For  $h \neq 0$ , we find four gapless modes for both the canted  $\mathrm{SLP}_1$  and the  $\mathrm{SLP}_{3,M}$  states. This is again in agreement with the number of independent solutions to the linearized normalization equations of the SLP ansatz in a field. While we expect that a higher order spin wave calculation will gap some of the modes, it is interesting to note that a particular nonlinear deformation of the spins should be expected to change the state according to what the interpolation parameter  $\alpha$  would do (see Appendix B), thus maintaining zero energy even for nonlinear changes. The striking difference between the dynamical structure factors of the  $SLP_1$  and  $SLP_{3,M}$  states is that the latter shows more intermediate intensity spin wave branches. Yet, for neutron scattering experiments it might be more important that SLP<sub>1</sub> has high-intensity low-energy longitudinal spin waves, while  $SLP_{3,M}$  only has transverse.

Higher order spin wave calculations should be able to describe magnon decays caused by cubic bosonic terms, which generally occur for non-collinear ground states [44, 45]. For a future study, it would be interesting to investigate how this affects the  $\mathrm{SLP}_1$  and  $\mathrm{SLP}_{3,M}$  spin wave spectra.

The  $J_1$ - $J_{3b}$  model studied here is believed to be relevant for the  $Gd_2B_2O_7$  class of materials (B is a nonmagnetic cation) [25], however with additional dipoledipole interactions [46-48]. While we have not considered dipole-dipole interactions, it would be interesting to study the effects of these and other interactions on our results. We note that other Heisenberg interactions were investigated in the zero-field case in Ref. 8. There, the  $SLP_1$  state survives when adding  $J_2$  and  $J_{3a}$  as long as  $J_1 > J_{3b}$  are both larger than  $J_{3a} - J_2$ . Particularly, it would be interesting to study the stability of the collinear SLP-X phase found close to  $J_{3b} = J_{3a} - J_2$ , and possible multi- $\vec{Q}$  SLP<sub>3</sub> analogs of this phase. This would be relevant for pyrochlore spinel materials [26, 27] and the breathing pyrochlore materials LiGaCr<sub>4</sub>O<sub>8</sub> and LiInCr<sub>4</sub>O<sub>8</sub> [49]. As most of our results rely on satisfying

the tetrahedron and triangle conditions, we expect that the accurate values of  $J_1$  and  $J_{3b}$  are not important as long as they are both AF. Therefore, our results should apply also to breathing pyrochlores.

We hope that this work can lead to experimental searches for multi- $\vec{Q}$  ordered phases in pyrochlore magnets, and also inspire theoretical investigations of other 3D models of frustrated magnetism.

#### ACKNOWLEDGMENTS

We thank Michel Gingras for useful discussions and Claudio Castelnovo for directing us towards the  $J_1$ - $J_{3b}$  model. C.G. acknowledges funding from the Aker Scholarship. The computations were performed on resources provided by Sigma2 - the National Infrastructure for High Performance Computing and Data Storage in Norway, and on the Fox supercomputer at the University of Oslo.

#### Appendix A: Length constraints

In a proper classical state, each spin must have unit length. Inserting  $\vec{R} = n_1 \vec{a}_1 + n_2 \vec{a}_2 + n_3 \vec{a}_3$  and values for  $\vec{Q}_{ij}$  from Table I into the SLP ansatz Eq. (7), we find for sublattice zero

$$\begin{split} \vec{S}_{0,\vec{R}} &= \vec{u}_{01} \cos{(\frac{2\pi}{3}(n_3 - n_2))} + \vec{v}_{01} \sin{(\frac{2\pi}{3}(n_3 - n_2))} \\ &+ \vec{u}_{02} \cos{(\frac{2\pi}{3}(n_1 - n_3))} + \vec{v}_{02} \sin{(\frac{2\pi}{3}(n_1 - n_3))} \\ &+ \vec{u}_{03} \cos{(\frac{2\pi}{3}(n_2 - n_1))} + \vec{v}_{02} \sin{(\frac{2\pi}{3}(n_2 - n_1))} + \vec{m}. \end{split}$$

Setting  $k \equiv n_3 - n_2$ ,  $l \equiv n_1 - n_3$  and  $m \equiv n_2 - n_1$ , we see that k + l + m = 0. The  $2\pi/3$  factor means that the integers k, l, m should be understood modulo three. Thus the SLP ansatz imply in all nine different spin possibilities on sublattice zero (k and l can take three independent values each, and m then follows). The nine spins in the notation  $\vec{S}_{0,klm}$  are

$$\begin{split} \vec{S}_{0,000} &= \vec{u}_{01} + \vec{u}_{02} + \vec{u}_{03} + \vec{m}, \\ \vec{S}_{0,\pm(111)} &= \frac{1}{2} \left( -\vec{u}_{01} - \vec{u}_{02} - \vec{u}_{03} + 2\vec{m} \right) \pm \frac{\sqrt{3}}{2} \left( \vec{v}_{01} + \vec{v}_{02} + \vec{v}_{03} \right), \\ \vec{S}_{0,\pm(01-1)} &= \frac{1}{2} \left( 2\vec{u}_{01} - \vec{u}_{02} - \vec{u}_{03} + 2\vec{m} \right) \pm \frac{\sqrt{3}}{2} \left( \vec{v}_{02} - \vec{v}_{03} \right), \\ \vec{S}_{0,\pm(-101)} &= \frac{1}{2} \left( 2\vec{u}_{02} - \vec{u}_{03} - \vec{u}_{01} + 2\vec{m} \right) \pm \frac{\sqrt{3}}{2} \left( \vec{v}_{03} - \vec{v}_{01} \right), \\ \vec{S}_{0,\pm(1-10)} &= \frac{1}{2} \left( 2\vec{u}_{03} - \vec{u}_{01} - \vec{u}_{02} + 2\vec{m} \right) \pm \frac{\sqrt{3}}{2} \left( \vec{v}_{01} - \vec{v}_{02} \right). \end{split}$$

Repeating this for the other sublattices, we find in total 36 length constraint equations:

 $(\vec{u}_{01} + \vec{u}_{02} + \vec{u}_{03} + \vec{m})^2 = 1,$ 

 $(\vec{u}_{01} - \vec{u}_{12} - \vec{u}_{13} - \vec{m})^2 = 1.$ 

$$(\vec{u}_{02} + \vec{u}_{12} - \vec{u}_{23} - \vec{m})^2 = 1,$$

$$(\vec{u}_{03} + \vec{u}_{13} + \vec{u}_{23} - \vec{m})^2 = 1,$$

$$(\vec{u}_{01} + \vec{u}_{02} + \vec{u}_{03} - 2\vec{m})^2 + 3 (\vec{v}_{01} + \vec{v}_{02} + \vec{v}_{03})^2 = 4,$$

$$(\vec{u}_{01} - \vec{u}_{12} - \vec{u}_{13} + 2\vec{m})^2 + 3 (\vec{v}_{01} + \vec{v}_{12} - \vec{v}_{13})^2 = 4,$$

$$(\vec{u}_{02} + \vec{u}_{12} - \vec{u}_{23} + 2\vec{m})^2 + 3 (\vec{v}_{02} + \vec{v}_{12} + \vec{v}_{23})^2 = 4,$$

$$(\vec{u}_{02} + \vec{u}_{12} - \vec{u}_{23} + 2\vec{m})^2 + 3 (\vec{v}_{02} + \vec{v}_{12} + \vec{v}_{23})^2 = 4,$$

$$(\vec{u}_{03} + \vec{u}_{13} + \vec{u}_{23} + 2\vec{m})^2 + 3 (\vec{v}_{03} - \vec{v}_{13} + \vec{v}_{23})^2 = 4,$$

$$(2\vec{u}_{01} - \vec{u}_{02} - \vec{u}_{03} + 2\vec{m})^2 + 3 (\vec{v}_{02} - \vec{v}_{03})^2 = 4,$$

$$(\vec{u}_{01} - 2\vec{u}_{02} + \vec{u}_{03} - 2\vec{m})^2 + 3 (\vec{v}_{01} - \vec{v}_{02})^2 = 4,$$

$$(\vec{u}_{01} + \vec{u}_{02} - 2\vec{u}_{03} - 2\vec{m})^2 + 3 (\vec{v}_{11} + \vec{v}_{13})^2 = 4,$$

$$(\vec{u}_{01} + \vec{u}_{12} + \vec{u}_{13} - 2\vec{m})^2 + 3 (\vec{v}_{01} - \vec{v}_{02})^2 = 4,$$

$$(\vec{u}_{01} + 2\vec{u}_{12} - \vec{u}_{13} + 2\vec{m})^2 + 3 (\vec{v}_{01} + \vec{v}_{13})^2 = 4,$$

$$(\vec{u}_{01} + 2\vec{u}_{12} - \vec{u}_{13} + 2\vec{m})^2 + 3 (\vec{v}_{01} - \vec{v}_{12})^2 = 4,$$

$$(\vec{u}_{01} - \vec{u}_{12} + 2\vec{u}_{13} + 2\vec{m})^2 + 3 (\vec{v}_{01} - \vec{v}_{12})^2 = 4,$$

$$(\vec{u}_{02} - \vec{u}_{12} + \vec{u}_{23} - 2\vec{m})^2 + 3 (\vec{v}_{02} - \vec{v}_{23})^2 = 4,$$

$$(\vec{u}_{02} - \vec{u}_{12} + \vec{u}_{23} + 2\vec{m})^2 + 3 (\vec{v}_{02} - \vec{v}_{23})^2 = 4,$$

$$(\vec{u}_{02} - \vec{u}_{13} + \vec{u}_{23} - 2\vec{m})^2 + 3 (\vec{v}_{02} - \vec{v}_{23})^2 = 4,$$

$$(\vec{u}_{03} - \vec{u}_{13} - \vec{u}_{23} - 2\vec{m})^2 + 3 (\vec{v}_{03} - \vec{v}_{23})^2 = 4,$$

$$(\vec{u}_{03} - \vec{u}_{13} - \vec{u}_{23} - 2\vec{m})^2 + 3 (\vec{v}_{03} - \vec{v}_{23})^2 = 4,$$

$$(\vec{u}_{03} + \vec{u}_{13} - \vec{u}_{23} - 2\vec{m})^2 + 3 (\vec{v}_{03} - \vec{v}_{13})^2 = 4,$$

$$(\vec{u}_{01} + \vec{u}_{02} + \vec{u}_{03} - 2\vec{m}) \cdot (\vec{v}_{01} + \vec{v}_{02} + \vec{v}_{03}) = 0,$$

$$(\vec{u}_{01} + \vec{u}_{02} + \vec{u}_{03} - 2\vec{m}) \cdot (\vec{v}_{01} + \vec{v}_{02} + \vec{v}_{03}) = 0,$$

$$(\vec{u}_{01} + \vec{u}_{02} + \vec{u}_{03} - 2\vec{m}) \cdot (\vec{v}_{01} + \vec{v}_{02} + \vec{v}_{03}) = 0,$$

$$(\vec{u}_{01} + \vec{u}_{12} - \vec{u}_{13} + 2\vec{m}) \cdot (\vec{v}_{01} - \vec{v}_{0$$

 $(\vec{u}_{01} - \vec{u}_{12} + 2\vec{u}_{13} + 2\vec{m}) \cdot (\vec{v}_{01} - \vec{v}_{12}) = 0,$ 

 $(2\vec{u}_{02} - \vec{u}_{12} + \vec{u}_{23} - 2\vec{m}) \cdot (\vec{v}_{12} - \vec{v}_{23}) = 0,$ 

 $(\vec{u}_{02} - 2\vec{u}_{12} - \vec{u}_{23} + 2\vec{m}) \cdot (\vec{v}_{02} - \vec{v}_{23}) = 0,$ 

 $(\vec{u}_{02} + \vec{u}_{12} + 2\vec{u}_{23} + 2\vec{m}) \cdot (\vec{v}_{02} - \vec{v}_{12}) = 0,$ 

 $(2\vec{u}_{03} - \vec{u}_{13} - \vec{u}_{23} - 2\vec{m}) \cdot (\vec{v}_{13} + \vec{v}_{23}) = 0,$ 

 $(\vec{u}_{03} - 2\vec{u}_{13} + \vec{u}_{23} + 2\vec{m}) \cdot (\vec{v}_{03} - \vec{v}_{23}) = 0,$  $(\vec{u}_{03} + \vec{u}_{13} - 2\vec{u}_{23} + 2\vec{m}) \cdot (\vec{v}_{03} + \vec{v}_{13}) = 0.$ 

Appendix B: 
$$SLP_{3,\alpha}$$

The  $\mathrm{SLP}_{3,\alpha}$  family of ground states interpolates smoothly between  $\mathrm{SLP}_1$  at  $\alpha=0$  and  $\mathrm{SLP}_{3,M}$  at  $\alpha=\alpha_{max}$ . Here, we give explicit expressions for the  $\vec{u}$ 's and  $\vec{v}$ 's of  $\mathrm{SLP}_{3,\alpha}$  when the magnetic field is in the z-direction. We have chosen  $\vec{u}_{01}$  to be along  $\hat{x}$ . With  $a=(1-m^2-8m^2\tan^2\alpha)/2$  and  $b=((1-m^2)^2-16m^2(1+3m^2)\tan^2\alpha)^{1/2}/2$ , the  $\mathrm{SLP}_{3,\alpha}$  state is given by

$$\begin{split} \vec{u}_{01} &= \sqrt{a+b} \, (1,0,0), & \vec{v}_{01} &= |\vec{u}_{01}| (0,-1,0), \\ \vec{u}_{02} &= (0,0,0), & \vec{v}_{02} &= 4m \tan \alpha \, (0,0,-1), \\ \vec{u}_{03} &= \sqrt{a-b} \, (\sin \alpha, \cos \alpha,0), & \vec{v}_{03} &= |\vec{u}_{03}| (-\cos \alpha, \sin \alpha,0), \\ u_{12}^{xy} &= -u_{03}^{xy}, \ u_{12}^z &= u_{03}^z, & v_{12}^{xy} &= v_{03}^z, \ v_{12}^z &= -v_{03}^z, \\ u_{13}^{xy} &= -u_{02}^{xy}, \ u_{13}^z &= u_{02}^z, & v_{13}^{xy} &= -v_{02}^{xy}, \ v_{13}^z &= v_{02}^z, \\ u_{23}^{xy} &= u_{01}^{y}, \ u_{23}^z &= 0, & v_{23}^{xy} &= v_{01}^{y}, \ v_{23}^z &= 0. \end{split}$$

Setting  $\alpha = 0$  one obtains the canted SLP<sub>1</sub> state. In the opposite limit, for  $\alpha = \alpha_{max}$ , we get the SLP<sub>3,M</sub> state:

$$\begin{split} \vec{u}_{01} &= \frac{c_7 c_{-1}}{2 c_3} (1,0,0), \qquad \vec{v}_{01} &= |\vec{u}_{01}| (0,-1,0), \\ \vec{u}_{02} &= (0,0,0), \qquad & \vec{v}_{02} &= \frac{c_{-1}^2}{c_3} (0,0,-1), \\ \vec{u}_{03} &= \frac{c_{-1}}{c_7} (\frac{c_{-1}^2}{2 c_3},2m,0), \quad \vec{v}_{03} &= \frac{c_{-1}}{c_7} (-2m,\frac{c_{-1}^2}{2 c_3},0), \end{split}$$

where we have used the abbreviations  $c_3 \equiv \sqrt{1+3m^2}$  and  $c_7 \equiv \sqrt{1+7m^2}$ .

For small  $\alpha$ , valid to  $\mathcal{O}(\alpha^2)$ , we get

$$\vec{u}_{01} = \left[ c_{-1} - \frac{4m^2c_1^2}{c_{-1}^3} \alpha^2 \right] (1,0,0), \quad \vec{v}_{01} = |\vec{u}_{01}|(0,-1,0),$$

$$\vec{u}_{02} = (0,0,0), \qquad \qquad \vec{v}_{02} = 4m\alpha(0,0,-1),$$

$$\vec{u}_{03} = \frac{4m^2\alpha}{c_{-1}} (\alpha,1,0), \qquad \qquad \vec{v}_{03} = \frac{4m^2\alpha}{c_{-1}} (-1,\alpha,0),$$

where we have used  $c_{-1} \equiv \sqrt{1 - m^2}$  and  $c_1 \equiv \sqrt{1 + m^2}$ .

#### Appendix C: Spin wave expansion

The spin wave expansion is carried out by first defining a rotated frame

$$S_{\vec{r}}^{\alpha} = R_{\vec{r}}^{\alpha\beta} S_{\vec{r}}^{\prime\beta}, \tag{C1}$$

such that a ferromagnetic spin configuration along the z-axis in the rotated frame is equal to the ground state spin configuration. In the rotated frame, we do a Holstein-Primakoff transformation [30] to expand around the ground state

$$\begin{pmatrix}
S_{\vec{r}}^{lx} \\
S_{\vec{r}}^{ly} \\
S_{\vec{r}}^{lz}
\end{pmatrix} = \begin{pmatrix}
\sqrt{\frac{S}{2}} \left( a_{\vec{r}}^{\dagger} + a_{\vec{r}} \right) \\
i\sqrt{\frac{S}{2}} \left( a_{\vec{r}}^{\dagger} - a_{\vec{r}} \right) \\
S - a_{\vec{r}}^{\dagger} a_{\vec{r}}
\end{pmatrix}.$$
(C2)

Inserting this into the Hamiltonian, the linear terms in boson operators vanish, and the quadratic part of the Hamiltonian becomes

$$H = \frac{1}{2} \sum_{\vec{q}} \Phi_{\vec{q}}^{\dagger} H_{\vec{q}} \Phi_{\vec{q}}, \tag{C3}$$

where  $\vec{q}$  runs over the first Brillouin zone of the lattice with an unit cell of  $M=4\times 3^3=108$  spins.  $\Phi_{\vec{q}}=[a_{\vec{q},1},\cdots,a_{\vec{q},M},a_{-\vec{q},1}^{\dagger},\cdots,a_{-\vec{q},M}^{\dagger}]^T$  is a 2M column vector of boson operators, and  $H_{\vec{q}}$  is a  $2M\times 2M$  matrix with coefficients coming from both the rotation matrices and the parameters of the original Hamiltonian.

Being boson operators, the components of  $\Phi_{\vec{q}}$  must obey the commutation relations

$$\left[\Phi_{\vec{q},i}, \Phi_{\vec{q},j}^{\dagger}\right] = g_{ij}, \tag{C4}$$

where g is a diagonal  $2M \times 2M$  matrix with +1 (-1) on the upper (lower) M entries. To diagonalize the Hamiltonian, we define transformed bosons  $\Psi$  in the following way

$$\Phi_{\vec{q}} = T_{\vec{q}} \Psi_{\vec{q}},\tag{C5}$$

where  $T_{\vec{q}}$  is a  $2M \times 2M$  matrix and  $\Psi_{\vec{q}}$  is a 2M column vector of transformed boson operators that also obey the commutation relations Eq. (C4). This requirement leads to the following restriction on  $T_{\vec{q}}$ 

$$T_{\vec{q}} g T_{\vec{q}}^{\dagger} = g. \tag{C6}$$

To diagonalize  $H_{\vec{q}}$  while maintaining this restriction, we follow Colpa [31] and decompose  $H_{\vec{q}}$  using a Cholesky decomposition  $H_{\vec{q}} = K_{\vec{q}}^{\dagger} K_{\vec{q}}$ . Then the Hermitian matrix  $K_{\vec{q}}gK_{\vec{q}}^{\dagger}$  is diagonalized, and its eigenvalues are sorted in descending order and assigned to the diagonal matrix  $D_{\vec{q}}$ . We denote by  $U_{\vec{q}}$  the corresponding unitary matrix with eigenvectors of  $K_{\vec{q}}gK_{\vec{q}}^{\dagger}$  as columns. It then follows that

$$T_{\vec{q}} = K_{\vec{q}}^{-1} U_{\vec{q}} \sqrt{g D_{\vec{q}}}, \tag{C7}$$

which satisfies Eq. (C6). The diagonal matrix of energy eigenvalues is

$$E_{\vec{q}} = T_{\vec{q}}^{\dagger} H_{\vec{q}} T_{\vec{q}} = g D_{\vec{q}}. \tag{C8}$$

Thus, the spin wave frequencies at  $+\vec{q}$  can be read off from the upper M entries of gD:

$$\omega_{\vec{q},i} = D_{\vec{q}}^{ii}. \tag{C9}$$

This (para)diagonalization procedure fails if  $H_{\vec{q}}$  is not positive definite. Therefore, we add a small positive constant diagonal matrix to  $H_{\vec{q}}$  to keep the eigenvalues positive

The dynamical structure factor is defined as

$$S^{\mu\nu}(\vec{q},\omega) = \int_{-\infty}^{\infty} dt \sum_{\vec{r},\vec{r}'} \langle S^{\mu}_{\vec{r}}(t) S^{\nu}_{\vec{r}'}(0) \rangle e^{-i\vec{q}\cdot(\vec{r}-\vec{r}')} e^{i\omega t}.$$
(C10)

Inserting the rotation matrices and performing the Holstein-Primakoff transformation, keeping at most terms that are quadratic in the transformed boson operators, one can evaluate the boson correlators at zero temperature. Writing the transformation matrix  $T_{\vec{q}}$  on block-matrix form

$$T_{\vec{q}} = \begin{pmatrix} A_{\vec{q}} & B_{\vec{q}} \\ C_{\vec{q}} & D_{\vec{q}} \end{pmatrix} \tag{C11}$$

and defining  $\tilde{A}^{ij}_{\vec{q}} \equiv e^{-i\vec{q}\cdot\vec{\alpha}_i}A^{ij}$  and  $\tilde{C}^{ij}_{\vec{q}} \equiv e^{-i\vec{q}\cdot\vec{\alpha}_i}C^{ij}$ , where  $\vec{\alpha}_i$  is the position of the *i*'th spin inside the unit cell, we arrive at the following expression for the dynamical structure factor

$$S^{\mu\nu}(\vec{q},\omega) = \pi NS \sum_{i=1}^{M} \delta(\omega - \omega_{\vec{q},j}) \times$$
 (C12)

$$\sum_{i,i'}^{M} \left[ \tilde{A}_{\vec{q}}^{\dagger ji'} \left( R_{i'} \Lambda_1^* R_i^T \right)^{\nu \mu} \tilde{A}_{\vec{q}}^{ij} + \tilde{C}_{\vec{q}}^{\dagger ji'} \left( R_{i'} \Lambda_1 R_i^T \right)^{\nu \mu} \tilde{C}_{\vec{q}}^{ij} \right]$$

$$\left. + \tilde{A}_{\vec{q}}^{\dagger j i'} \left( R_{i'} \Lambda_2 R_i^T \right)^{\nu \mu} \tilde{C}_{\vec{q}}^{ij} + \tilde{C}_{\vec{q}}^{\dagger j i'} \left( R_{i'} \Lambda_2^* R_i^T \right)^{\nu \mu} \tilde{A}_{\vec{q}}^{ij} \right],$$

where

$$\Lambda_1 = \begin{pmatrix} 1 & i & 0 \\ -i & 1 & 0 \\ 0 & 0 & 0 \end{pmatrix}, \quad \Lambda_2 = \begin{pmatrix} 1 & i & 0 \\ i & -1 & 0 \\ 0 & 0 & 0 \end{pmatrix}.$$

# Appendix D: Entropy for h=0 solutions

In zero magnetic field, the ground states are parametrized by three unit vectors:  $\vec{u}_{01}, \vec{w}_1$  and  $\vec{w}_2$ , where  $\vec{u}_{01}$  is perpendicular to  $\vec{w}_1$  and  $\vec{w}_2$ . We label the angle between  $\vec{w}_1$  and  $\vec{w}_2$  as  $\theta$ . Then, computing the entropy for these solutions using spin waves, we get the results shown in Fig. 14. The maximal entropy occurs for  $\theta = \pi$ , which corresponds to the coplanar SLP<sub>1</sub> solution.

For the zero-field  $SLP_{3,M}$  state, we find eight gapless modes, compared to 14 for the coplanar  $SLP_1$  state. Thus, we conclude that the coplanar  $SLP_1$  solution also has higher entropy than the zero-field  $SLP_{3,M}$  state.

## Appendix E: SLP order parameter

The SLP order parameter measures the staggered magnetization on chains along  $\vec{a}_i - \vec{a}_j$ :

$$\vec{C}_{\vec{R}_{0},ij} \equiv \frac{1}{2L} \sum_{n} \left( \vec{S}_{\vec{R}_{0}+n(\vec{a}_{j}-\vec{a}_{i}),i} - \vec{S}_{\vec{R}_{0}+n(\vec{a}_{j}-\vec{a}_{i}),j} \right),$$
(E1)

where  $\vec{R}_0$  is an arbitrary up tetrahedron on the chain. Inserting the SLP ansatz, and performing the sum over n, trigonometric terms with arguments  $2\pi n/3$  sum to zero (for L divisible by 3). The only surviving terms

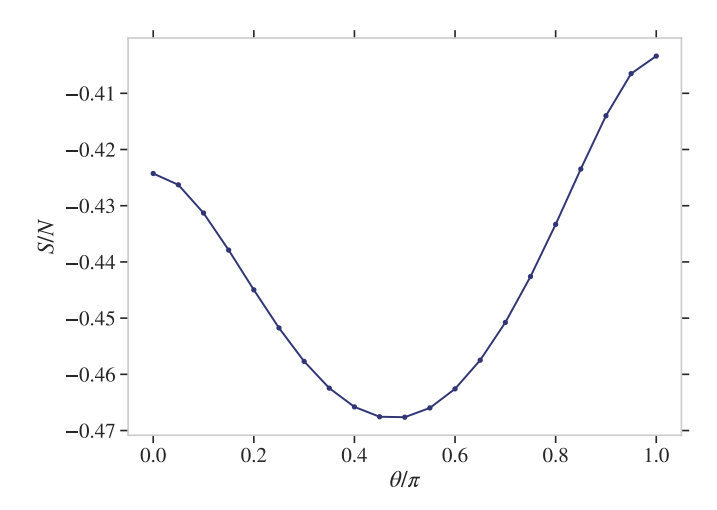


FIG. 14. The entropy for the h = 0 solution characterized by the angle  $\theta$  between the two vectors  $\vec{w}_1$  and  $\vec{w}_2$ .

are those with  $\vec{Q}_{ij}$  which follows from the fact that  $\vec{Q}_{ij} \cdot (\vec{a}_i - \vec{a}_j) = 0 \mod 2\pi$ , ensuring that each term in the sum is independent of n. This gives

$$\vec{C}_{\vec{R}_0,ij} = \vec{u}_{ij}\cos(\vec{Q}_{ij}\cdot\vec{R}_0) + \vec{v}_{ij}\sin(\vec{Q}_{ij}\cdot\vec{R}_0).$$
 (E2)

We then square this and take the average over all parallel chains. This is achieved by summing over all points on the fcc Bravais lattice

$$C_{ij}^2 = \frac{1}{L^3} \sum_{\vec{R}_0} \left( \vec{u}_{ij} \cos(\vec{Q}_{ij} \cdot \vec{R}_0) + \vec{v}_{ij} \sin(\vec{Q}_{ij} \cdot \vec{R}_0) \right)^2.$$
(E5)

Performing this average, the trigonometric terms reduce to

$$\frac{1}{L^3} \sum_{\vec{R}_0} \cos^2(\vec{Q}_{ij} \cdot \vec{R}_0) = \frac{1}{2},\tag{E4}$$

$$\frac{1}{L^3} \sum_{\vec{R}_0} \sin^2(\vec{Q}_{ij} \cdot \vec{R}_0) = \frac{1}{2},\tag{E5}$$

$$\frac{1}{L^3} \sum_{\vec{R}_0} \cos(\vec{Q}_{ij} \cdot \vec{R}_0) \sin(\vec{Q}_{ij} \cdot \vec{R}_0) = 0, \quad (E6)$$

implying that

$$C_{ij}^2 = \frac{1}{2} \left( \vec{u}_{ij}^2 + \vec{v}_{ij}^2 \right).$$
 (E7)

Now by considering the length constraint equations for the spins on sublattice zero, one can show that they imply

$$\vec{u}_{01}^2 + \vec{v}_{01}^2 + \vec{u}_{02}^2 + \vec{v}_{02}^2 + \vec{v}_{03}^2 + \vec{v}_{03}^2 = 2(1 - \vec{m}^2).$$
 (E8)

Similar relations can be obtained for the other sublattices. Adding and subtracting these relations it follows that

$$\vec{u}_{01}^2 + \vec{v}_{01}^2 = \vec{u}_{23}^2 + \vec{v}_{23}^2, \tag{E9}$$

which implies  $C_{23} = C_{01}$ . Similarly  $C_{13} = C_{02}$  and  $C_{12} = C_{03}$ . Therefore the three component complex order parameter, which captures also other sublattice pairings

$$O_{\rm SLP} = C_{01}C_{23} + e^{i2\pi/3}C_{02}C_{13} + e^{i4\pi/3}C_{03}C_{12}$$

becomes

$$\begin{split} O_{\rm SLP} &= C_{01}^2 + e^{i2\pi/3} C_{02}^2 + e^{i4\pi/3} C_{03}^2 \\ &= C_{01}^2 - \frac{1}{2} (C_{02}^2 + C_{03}^2) + \frac{\sqrt{3}}{2} i \left( C_{02}^2 - C_{03}^2 \right). \end{split}$$

Squaring gives

$$|O_{\text{SLP}}|^2 = \left(C_{01}^2 - \frac{1}{2}(C_{02}^2 + C_{03}^2)\right)^2 + \frac{3}{4}\left(C_{02}^2 - C_{03}^2\right)^2$$

$$= \left(C_{01}^2 + C_{02}^2 + C_{03}^2\right)^2 - 3\left(C_{01}^2 C_{02}^2 + C_{01}^2 C_{03}^2 + C_{02}^2 C_{03}^2\right)$$
Using Eq. (E8), we get

$$|O_{\text{SLP}}| = \sqrt{(1 - \vec{m}^2)^2 - 3(C_{01}^2 C_{02}^2 + C_{01}^2 C_{03}^2 + C_{02}^2 C_{03}^2)}.$$

## Appendix F: Two wave vectors on a sublattice

We show in this section that the spins in an SLP state with two wave vectors on a sublattice, SLP<sub>2</sub>, cannot be normalized. Setting  $\vec{u}_{03} = \vec{v}_{03} = 0$ , the nine sublattice zero equations reduce to:

$$(\vec{u}_{01} + \vec{u}_{02} + \vec{m})^2 = 1,$$
 (F1)

$$(\vec{u}_{01} + \vec{u}_{02} - 2\vec{m})^2 + 3(\vec{v}_{01} + \vec{v}_{02})^2 = 4,$$
 (F2)

$$(-2\vec{u}_{01} + \vec{u}_{02} - 2\vec{m})^2 + 3\vec{v}_{02}^2 = 4,$$
 (F3)

$$(\vec{u}_{01} - 2\vec{u}_{02} - 2\vec{m})^2 + 3\vec{v}_{01}^2 = 4,$$
 (F4)

$$(\vec{u}_{01} + \vec{u}_{02} - 2\vec{m})^2 + 3(\vec{v}_{01} - \vec{v}_{02})^2 = 4,$$
 (F5)

$$(\vec{u}_{01} + \vec{u}_{02} - 2\vec{m}) \cdot \vec{v}_{01} = 0, \tag{F6}$$

$$(\vec{u}_{01} + \vec{u}_{02} - 2\vec{m}) \cdot \vec{v}_{02} = 0, \tag{F7}$$

$$(\vec{u}_{01} - 2\vec{u}_{02} - 2\vec{m}) \cdot \vec{v}_{01} = 0, \tag{F8}$$

$$(-2\vec{u}_{01} + \vec{u}_{02} - 2\vec{m}) \cdot \vec{v}_{02} = 0.$$
 (F9)

Eqs. (F2) and (F5) can be combined to give

$$\vec{v}_{01} \cdot \vec{v}_{02} = 0,$$
 (F10)

and the sum of Eqs. (F3) and (F4) combined with Eq. (F1) gives

$$\vec{u}_{01} \cdot \vec{u}_{02} = 0. \tag{F11}$$

If we now consider the planes spanned by these  $\vec{u}$ 's and  $\vec{v}$ 's, it follows from the orthogonality conditions that  $(\vec{u}_{01} + \vec{u}_{02} - 2\vec{m})$  is a normal vector for the  $\vec{v}$ -plane. The remaining orthogonality conditions then give

$$\vec{u}_{01} \cdot \vec{v}_{02} = 0, \tag{F12}$$

$$\vec{u}_{02} \cdot \vec{v}_{01} = 0. \tag{F13}$$

The remaining length constraints give that

$$\vec{u}_{01}^2 + 4\vec{u}_{01} \cdot \vec{m} = \vec{v}_{01}^2, \tag{F14}$$

$$\vec{u}_{02}^2 + 4\vec{u}_{02} \cdot \vec{m} = \vec{v}_{02}^2, \tag{F15}$$

and

$$\vec{u}_{01}^2 + \vec{u}_{02}^2 + 2(\vec{u}_{01} + \vec{u}_{02}) \cdot \vec{m} = 1 - m^2.$$
 (F16)

In zero magnetic field  $(\vec{m} = 0)$ , it is consequently impossible to normalize the spins. This is because  $(\vec{u}_{01} + \vec{u}_{02})$ 

is the normal vector to the  $\vec{v}$ -plane (none of the vectors can have zero length, as that removes the corresponding  $\vec{Q}$  because  $\vec{u}_{01}^2 = \vec{v}_{01}^2$  and  $\vec{u}_{02}^2 = \vec{v}_{02}^2$ ). As  $\vec{v}_{02}$  is perpendicular to  $\vec{u}_{01}$  in addition to the  $\vec{v}$ -plane normal vector  $(\vec{u}_{01} + \vec{u}_{02})$ ,  $\vec{v}_{02}$  has to be normal to the  $\vec{v}$ -plane. However, as  $\vec{v}_{01}$  is normal to  $\vec{v}_{02}$  it follows that  $\vec{v}_{01}$  lies in the  $\vec{v}$ -plane, but that breaks the condition that  $(\vec{u}_{01} + \vec{u}_{02})$  is normal to the  $\vec{v}$ -plane. The same conclusion holds also in the presence of a magnetic field as we have verified by direct insertion into the length constraint equations on all sublattices using Mathematica<sup>TM</sup>.

- J. Villain, Insulating spin glasses, Zeitschrift für Physik B Condensed Matter 33, 31 (1979).
- [2] J. N. Reimers, A. J. Berlinsky, and A.-C. Shi, Mean-field approach to magnetic ordering in highly frustrated pyrochlores, Phys. Rev. B 43, 865 (1991).
- [3] J. N. Reimers, Absence of long-range order in a threedimensional geometrically frustrated antiferromagnet, Phys. Rev. B 45, 7287 (1992).
- [4] R. Moessner and J. T. Chalker, Properties of a Classical Spin Liquid: The Heisenberg Pyrochlore Antiferromagnet, Phys. Rev. Lett. 80, 2929 (1998).
- [5] G.-W. Chern, R. Moessner, and O. Tchernyshyov, Partial order from disorder in a classical pyrochlore antiferromagnet, Phys. Rev. B 78, 144418 (2008).
- [6] T. Okubo, T. H. Nguyen, and H. Kawamura, Cubic and noncubic multiple-q states in the Heisenberg antiferromagnet on the pyrochlore lattice, Phys. Rev. B 84, 144432 (2011).
- [7] M. Zhitomirsky, M. Gvozdikova, and T. Ziman, Noncoplanar multi-k states in frustrated spinel and kagome magnets, Annals of Physics 447, 169066 (2022).
- [8] C. Glittum and O. F. Syljuåsen, Sublattice pairing in pyrochlore Heisenberg antiferromagnets, Phys. Rev. B 108, 014413 (2023).
- [9] N. Nagaosa and Y. Tokura, Topological properties and dynamics of magnetic skyrmions, Nature Nanotechnology 8, 899 (2013).
- [10] W. Koshibae, Y. Kaneko, J. Iwasaki, M. Kawasaki, Y. Tokura, and N. Nagaosa, Memory functions of magnetic skyrmions, Japanese Journal of Applied Physics 54, 053001 (2015).
- [11] Y. Fujishiro, N. Kanazawa, T. Shimojima, A. Nakamura, K. Ishizaka, T. Koretsune, R. Arita, A. Miyake, H. Mitamura, K. Akiba, M. Tokunaga, J. Shiogai, S. Kimura, S. Awaji, A. Tsukazaki, A. Kikkawa, Y. Taguchi, and Y. Tokura, Large magneto-thermopower in MnGe with topological spin texture, Nature Communications 9, 408 (2018).
- [12] S. Mühlbauer, B. Binz, F. Jonietz, C. Pfleiderer, A. Rosch, Α. Neubauer, R. Georgii, and P. Böni, Skyrmion Lattice in a Chiral Magnet. Science **323**. 915 (2009).https://www.science.org/doi/pdf/10.1126/science.1166767.
- [13] S. D. Yi, S. Onoda, N. Nagaosa, and J. H. Han, Skyrmions and anomalous Hall effect in a Dzyaloshinskii-Moriya spiral magnet, Phys. Rev. B 80, 054416 (2009).

- [14] S. Buhrandt and L. Fritz, Skyrmion lattice phase in three-dimensional chiral magnets from Monte Carlo simulations, Phys. Rev. B 88, 195137 (2013).
- [15] T. Okubo, S. Chung, and H. Kawamura, Multiple-q States and the Skyrmion Lattice of the Triangular-Lattice Heisenberg Antiferromagnet under Magnetic Fields, Phys. Rev. Lett. 108, 017206 (2012).
- [16] A. O. Leonov and M. Mostovoy, Multiply periodic states and isolated skyrmions in an anisotropic frustrated magnet, Nature Communications 6, 8275 (2015).
- [17] S. Hayami, S.-Z. Lin, and C. D. Batista, Bubble and skyrmion crystals in frustrated magnets with easy-axis anisotropy, Phys. Rev. B 93, 184413 (2016).
- [18] S. Hayami, S.-Z. Lin, Y. Kamiya, and C. D. Batista, Vortices, skyrmions, and chirality waves in frustrated Mott insulators with a quenched periodic array of impurities, Phys. Rev. B 94, 174420 (2016).
- [19] I. Martin and C. D. Batista, Itinerant Electron-Driven Chiral Magnetic Ordering and Spontaneous Quantum Hall Effect in Triangular Lattice Models, Phys. Rev. Lett. 101, 156402 (2008).
- [20] R. Ozawa, S. Hayami, K. Barros, G.-W. Chern, Y. Motome, and C. D. Batista, Vortex Crystals with Chiral Stripes in Itinerant Magnets, Journal of the Physical Society of Japan 85, 103703 (2016), https://doi.org/10.7566/JPSJ.85.103703.
- [21] S. Hayami, R. Ozawa, and Y. Motome, Effective bilinearbiquadratic model for noncoplanar ordering in itinerant magnets, Phys. Rev. B 95, 224424 (2017).
- [22] G.-W. Chern, Noncoplanar Magnetic Ordering Driven by Itinerant Electrons on the Pyrochlore Lattice, Phys. Rev. Lett. 105, 226403 (2010).
- [23] K. Aoyama and H. Kawamura, Hedgehog-lattice spin texture in classical Heisenberg antiferromagnets on the breathing pyrochlore lattice, Phys. Rev. B 103, 014406 (2021).
- [24] K. Aoyama and H. Kawamura, Hedgehog lattice and field-induced chirality in breathing-pyrochlore Heisenberg antiferromagnets, Phys. Rev. B 106, 064412 (2022).
- [25] A. S. Wills, M. E. Zhitomirsky, B. Canals, J. P. Sanchez, P. Bonville, P. D. de Réotier, and A. Yaouanc, Magnetic ordering in Gd2Sn2O7: the archetypal Heisenberg pyrochlore antiferromagnet, Journal of Physics: Condensed Matter 18, L37 (2006).
- [26] A. N. Yaresko, Electronic band structure and exchange coupling constants in  $A\operatorname{Cr}_2X_4$  spinels ( $A = \operatorname{Zn}$ , Cd, Hg;  $X = \operatorname{O}$ , S, Se), Phys. Rev. B **77**, 115106 (2008).

- [27] C. Cheng, Long-range antiferromagnetic interactions in ZnFe<sub>2</sub>O<sub>4</sub> and CdFe<sub>2</sub>O<sub>4</sub>: Density functional theory calculations, Phys. Rev. B 78, 132403 (2008).
- [28] K. Penc, N. Shannon, and H. Shiba, Half-Magnetization Plateau Stabilized by Structural Distortion in the Antiferromagnetic Heisenberg Model on a Pyrochlore Lattice, Phys. Rev. Lett. 93, 197203 (2004).
- [29] H. Kawamura and S. Miyashita, Phase Transition of the Heisenberg Antiferromagnet on the Triangular Lattice in a Magnetic Field, Journal of the Physical Society of Japan 54, 4530 (1985), https://doi.org/10.1143/JPSJ.54.4530.
- [30] T. Holstein and H. Primakoff, Field Dependence of the Intrinsic Domain Magnetization of a Ferromagnet, Phys. Rev. 58, 1098 (1940).
- [31] J. Colpa, Diagonalization of the quadratic boson hamiltonian, Physica A: Statistical Mechanics and its Applications 93, 327 (1978).
- [32] B. Berg and M. Lüscher, Definition and statistical distributions of a topological number in the lattice O(3)  $\sigma$ -model, Nuclear Physics B **190**, 412 (1981).
- [33] Metropolis, Nicholas and Rosenbluth, Arianna W. and Rosenbluth, Marshall N. and Teller, Augusta H. and Teller, Edward, Equation of State Calculations by Fast Computing Machines, The Journal of Chemical Physics 21, 1087 (1953), https://pubs.aip.org/aip/jcp/articlepdf/21/6/1087/18802390/1087\_1\_online.pdf.
- [34] D. P. Landau and K. Binder, A Guide to Monte Carlo Simulations in Statistical Physics, 3rd ed. (Cambridge University Press, 2009).
- [35] U. Wolff, Collective Monte Carlo Updating for Spin Systems, Phys. Rev. Lett. 62, 361 (1989).
- [36] D. Hinzke and U. Nowak, Monte Carlo simulation of magnetization switching in a Heisenberg model for small ferromagnetic particles, Computer Physics Communications 121-122, 334 (1999), proceedings of the Europhysics Conference on Computational Physics CCP 1998.
- [37] J. D. Alzate-Cardona, D. Sabogal-Suárez, R. F. L. Evans, and E. Restrepo-Parra, Optimal phase space sampling for Monte Carlo simulations of Heisenberg spin systems, Journal of Physics: Condensed Matter 31, 095802 (2019).
- [38] R. H. Swendsen and J.-S. Wang, Replica Monte Carlo Simulation of Spin-Glasses, Phys. Rev. Lett. 57, 2607 (1986).

- [39] H. G. Katzgraber, S. Trebst, D. A. Huse, and M. Troyer, Feedback-optimized parallel tempering Monte Carlo, Journal of Statistical Mechanics: Theory and Experiment 2006, P03018 (2006).
- [40] D. H. Lee, J. D. Joannopoulos, J. W. Negele, and D. P. Landau, Discrete-Symmetry Breaking and Novel Critical Phenomena in an Antiferromagnetic Planar (XY) Model in Two Dimensions, Phys. Rev. Lett. 52, 433 (1984).
- [41] H. Kawamura, Spin-wave analysis of the antiferromagnetic plane rotator model on the triangular lattice–symmetry breaking in a magnetic field, Journal of the Physical Society of Japan 53, 2452 (1984), https://doi.org/10.1143/JPSJ.53.2452.
- [42] M. V. Gvozdikova, P.-E. Melchy, and M. E. Zhitomirsky, Magnetic phase diagrams of classical triangular and kagome antiferromagnets, Journal of Physics: Condensed Matter 23, 164209 (2011).
- [43] L. Seabra, T. Momoi, P. Sindzingre, and N. Shannon, Phase diagram of the classical Heisenberg antiferromagnet on a triangular lattice in an applied magnetic field, Phys. Rev. B 84, 214418 (2011).
- [44] A. L. Chernyshev and M. E. Zhitomirsky, Magnon decay in noncollinear quantum antiferromagnets, Phys. Rev. Lett. 97, 207202 (2006).
- [45] M. E. Zhitomirsky and A. L. Chernyshev, Colloquium: Spontaneous magnon decays, Rev. Mod. Phys. 85, 219 (2013).
- [46] N. P. Raju, M. Dion, M. J. P. Gingras, T. E. Mason, and J. E. Greedan, Transition to long-range magnetic order in the highly frustrated insulating pyrochlore antiferromagnet Gd<sub>2</sub>Ti<sub>2</sub>O<sub>7</sub>, Phys. Rev. B 59, 14489 (1999).
- [47] A. P. Ramirez, B. S. Shastry, A. Hayashi, J. J. Krajew-ski, D. A. Huse, and R. J. Cava, Multiple Field-Induced Phase Transitions in the Geometrically Frustrated Dipolar Magnet: Gd<sub>2</sub>Ti<sub>2</sub>O<sub>7</sub>, Phys. Rev. Lett. 89, 067202 (2002).
- [48] P. G. Welch, J. A. M. Paddison, M. D. Le, J. S. Gardner, W.-T. Chen, A. R. Wildes, A. L. Goodwin, and J. R. Stewart, Magnetic structure and exchange interactions in the Heisenberg pyrochlore antiferromagnet Gd<sub>2</sub>Pt<sub>2</sub>O<sub>7</sub>, Phys. Rev. B 105, 094402 (2022).
- [49] P. Ghosh, Y. Iqbal, T. Müller, R. T. Ponnaganti, R. Thomale, R. Narayanan, J. Reuther, M. J. P. Gingras, and H. O. Jeschke, Breathing chromium spinels: a showcase for a variety of pyrochlore Heisenberg Hamiltonians, npj Quantum Materials 4, 63 (2019).